Extended performance study of forward osmosis during wastewater reclamation: Quantification of fouling-based concentration polarization effects on the flux decline

Thanh-Tin Nguyen[a], Rusnang Syamsul Adha[a], Robert W. Field[b], In S. Kim[a*]

[a]Global Desalination Research Center (GDRC), School of Earth Sciences and Environmental Engineering, Gwangju Institute of Science and Technology, 123 Cheomdangwagi-ro, Buk-gu, Gwangju 61005, Korea

[b]Department of Mechanical and Civil Engineering, Faculty of Engineering and Environment, Northumbria University, United Kingdom

[a*] Corresponding author.

In S. Kim

Email: iskim@gist.ac.kr

Telephone: +82-62-715-2477

Fax: +82-62-715-2434

- Published as https://doi.org/10.1016/j.memsci.2020.118755

Abstract

The long-term performance of forward osmosis during simulated wastewater reclamation was investigated for 120 h operation with a focus upon the influence of flux on flux decline and the synergistic effect of fouling on concentration polarization. Our comprehensive investigation focused on different fluxes (25; 30; 34 LMH) for simulated wastewater containing either a high protein or a low protein fraction. Compared to an initial flux of 25 LMH, operation at an initial 34 LMH favored the formation of a thicker and more compact cake layer which resulted in significant increase in both cake structural parameter (four-fold) and cake layer enhanced concentration polarization (ten-fold). After 40 h operation without physical cleaning the additional effect of cake layer enhanced concentration polarization and fouling resistance consumed 25% of the total driving force; the significant internal concentration polarization still had the greatest impact. In contrast operation at the lower flux of 25 LMH generated less fouling with a lower cake structural parameter (119 μm). The resultant flux decline was only 3% in contrast to the 15-18% found for the higher flux of 34 LMH. For operation above an initial 30 LMH it was found that FO fouling became irreversible if the wastewater contained a high protein fraction. Overall for a thin film composite membrane and a wastewater with a foulant concentration of 160 mg/L an initial flux of 25 LMH is the recommended threshold; this is 25% less that the critical value determined in earlier short-term studies.

Keywords: Forward Osmosis; Water reclamation; Long-term operation; Flux decline pattern.

1. Introduction

To resolve the water scarcity issue, seawater desalination and wastewater reuse are two main ways to supply fresh water. Due to the limitation imposed by thermodynamics, further significant reductions in the energy consumption of seawater reverse osmosis (SWRO) will be modest. Thus the range of water production cost can be expected to remain relatively high at 0.5-2 USD/m^3 [1]. Consequently, either primary or secondary wastewater effluent could be feasible sources for water recovery and reuse [2]. Water cost depends on the purpose of usage i.e. direct/indirect potable or non-potable reuse, ranging from 0.4-1.26 USD/m^3 [2]. Pressure membrane filtration processes are generally applied for water reclamation. However, these processes entail a high energy demand due to the use of a transmembrane pressure generated by the pump, especially for reverse osmosis (RO). Additionally, when wastewater is directly entered into the RO process, the irreversible fouling is anticipated to occur [3]. Forward osmosis (FO) membrane is emerging as a feasible technology for water reuse due to its energy-efficient and apparently lower fouling potential [4]. For a discussion of the later, see [22]. Whilst several studies have focused on the stand-alone FO for reclaiming primary/secondary wastewater effluent [5] [6] [7], even for high strength wastewater [8] [9], the FO membrane can be integrated with other processes (RO, UF, MD) as a means of osmotic dilution to attain simultaneous water reclamation and desalination [10] [11] [12] [13].

Previous work has indicated the cellulose triacetate (CTA) FO membrane has a superior performance being less susceptible to fouling and with higher flux recovery (60-98%) [14] [15] compared to the TFC membrane (30-50%) [5] [16]. However, these works only investigated a single foulant model such as sodium alginate (ALG), bovine serum albumin (BSA), or humic acid (HA) [17] [18]. In practice, wastewater contains complex organic foulants i.e., protein, carbohydrate, and natural organic matters, which leads to severe fouling and thus hinder sustainable long-term operation. As previously reported, biopolymers are viable foulants inducing

irreversible fouling in the pressurized membrane-based water treatment process [19]. This has also been reported in a past study on FO-RO hybrid process-based direct potable reuse [20]. Another study that used secondary wastewater as feed in the long-term FO operation reported that there was continual irreversible fouling [21]. The degree of FO fouling, cake layer compaction, and fouling reversibility are strongly influenced by the initial water flux [16] [22] [23]. Other works have indicated that FO fouling is very complicated because a greater amount of fouling does not necessarily lead to a greater severity of fouling [24]. As a final comment it is noted that FO fouling not only causes a decrease in water flux, change in product quality but also the membrane is damaged by the consequential cleaning.

As the inherent drawback of the FO membranes are concentration polarizations (CPs) effect, including dilutive internal concentration polarization (ICP) inside the porous membrane and external concentration polarization (ECPs) on both feed and draw side [25], a study of the synergistic effect of fouling on concentration polarization is important. The CPs cause a decrease in effective driving force and this fact is attributed to both accumulation/concentration of solute in the feed solution and the dilution of draw solution in the porous layer [26]. Past studies have evaluated the effect of CPs on overall FO performance [26] [27] [28]. Whilst their findings indicated CPs became more serious as DS concentration increased, these effects may be mitigated to a certain extent with increasing cross-flow velocity (CFV) i.e., from 5.56 to 11.11 cm/s [27], from 2.11 to 36.40 cm/s [28]. It has been found that fouling diminished by elevating CFV i.e., from 10.7 cm/s (*Re*= 615) to 32.1 cm/s (*Re*= 1936) [11] or from 6 to 24 cm/s [29] ; however, this option will cause an increase in energy consumption [8] [30]. Although the effect of CPs has been analyzed for the FO membrane process, e.g. [27] [28], fewer studies have investigated their influence when fouling occurs. When a fouling cake layer is formed on the active layer surface, this hinders back-diffusion of the solution and results in an increase in osmotic concentration at the interface between cake layer and active layer (AL). For the RO process, this has been termed

cake-enhanced concentration polarization (C-ECP) [31]. Now, with regard to the FO process, this phenomenon can be labelled as cake-enhanced osmotic pressure (C-EOP) because the solute accumulation induced by the effect of reverse solute flux (RSF) gives an elevated level of osmotic pressure within the fouling layer. The C-ECP effect has been reported in several studies of FO membrane fouling [29] [32]. However, it is worth noting that their works did not quantify its extent. A recent study has introduced a layered model to describe mass transport for a FO membrane fouled [33]. This work provides a model to predict the performance of a fouled FO. In turn, their findings have critically mentioned the cake structural parameter (S_c), and the foulant pore hydraulic diameter (D_h) as vital parameters influencing both water and solute transport [33] [34]. However, the profile of CPs in the presence of fouling has not been quantified in these studies. Although an earlier study (with AL-FS configuration) has reported on the couple effects of dilutive ICP and of the fouling occurring on the active layer-facing the feed solution [26], this work did not quantify the effects of CPs and C-ECPs on overall FO performance. In summary, whilst the fouling-enhanced CP and the ICP self-compensation have been noted as having impacts on the overall productivity of the fouled membrane, little attention has been directed towards a quantitative evaluation of the synergistic outcome of CPs and C-ECPs on overall FO performance.

Given the research gaps indicated above, our current study focused on the following objectives: i) To investigate the CPs and fouling-induced flux decline patterns of the TFC FO membrane under different fluxes for long-term operation of 120h whilst additionally studying the effect of feed compositions (low/high protein fraction present in wastewater) on flux decline and fouling reversibility; and ii) To quantify the effects of CPs (ICP, ECPs), the fouling-induced cake-enhanced CP, and the fouling resistance on the performance of a TFC membrane. Not only does the current study characterize the fouling behaviors by determining morphology, thickness and functional group of fouling layer, but also it covers the calculation of cake structural parameter, and when appropriate the effect of cake-enhanced CP. Finally, correlations between factors i.e.,

fouling layer thickness, cake structural parameter, cake-enhanced CP, fouling resistance, and flux decline rate was explored. This work lays a good foundation for an understanding of transport phenomena and fouling in the FO process, and also provides a guide for operation of the FO system.

2. Theory

A layered model has been developed to describe mass transport for a fouled FO membrane [33]. As foulants are deposited on the active layer surface, this will result in increasing solute concentration at the interface between the active layer and cake layer; this effect has been labelled as cake-enhanced CP [29] [32]. Briefly, the effects of ICP, ECPs (concentrative ECP in the feed side and dilutive ECP in draw side), and cake layer-enhanced CP phenomenon are presented in Fig. 1.

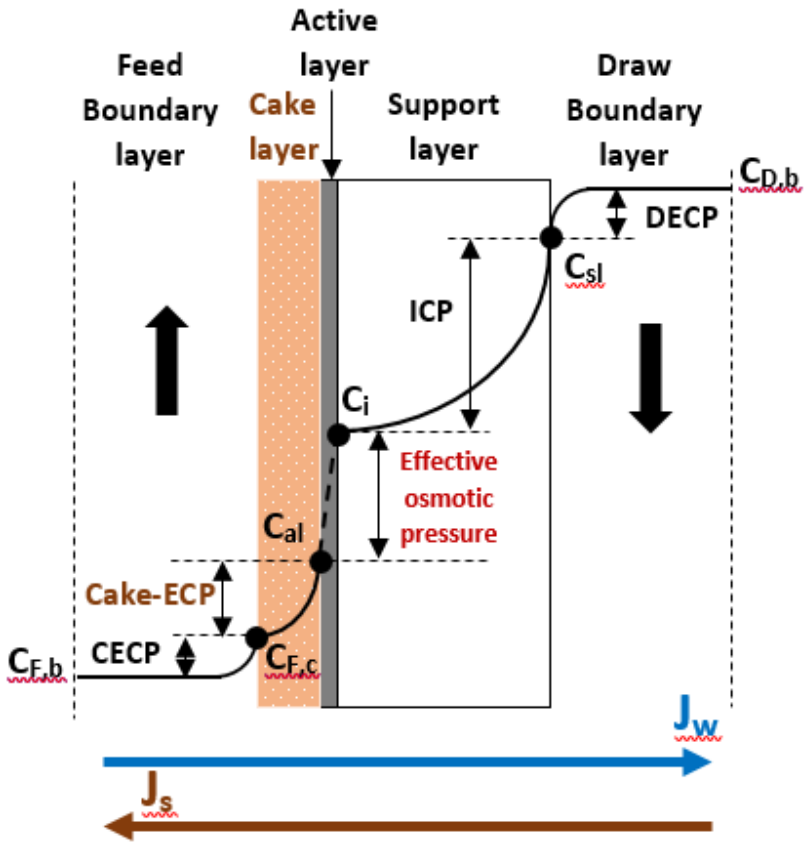

Figure 1. Schematic representation of solute concentration profiles across a fouled membrane under FO mode. ICP, ECPs, and cake-enhanced CP phenomena are accounted for the support

layer, boundary layers, and inside the foulant cake layer, respectively. The co-ordinate *x* is positive in the direction of positive J_w.

2.1. Internal concentration polarization

Conceptually, the transport of solute in the support layer include two solute fluxes in opposite directions: a diffusive flux ($D_S dC/dx$) and a convective flux ($J_w C$) [28].

$$J_w C + J_s = D_s \frac{dC}{dx} \quad (1)$$

where J_s is the reverse draw solute flux. J_w is the water flux, C is solute concentration, and D_s is an 'effective' solute diffusion coefficient for the support layer taking into account the porosity and tortuosity of the support. As commonly accepted, D_s is calculated from:

$$D_s = \frac{D_D \varepsilon}{\tau} \quad (2)$$

where D_D is the draw bulk diffusion coefficient, ε is the porosity of the support layer, and τ is the tortuosity of the support layer.

It has been noted that ICP occurring in the support layer decreases water permeation significantly across the membrane. Under FO mode (AL-FS), dilutive ICP causes a reduction in the osmotic pressure gradient across the active layer and thus a reduction in the water flux [26]. The boundary condition in the support layer is defined as Eq. (3).

$$\begin{cases} x = 0, C = C_i \\ x = l_{eff}, C = C_{sl} \end{cases} \quad (3)$$

where C_i is the solute concentration at the interface between the active layer and support layer, C_{sl} is the solute concentration on the membrane surface of the support layer, l_{eff} is the effective thickness of the support layer, which is regarded as the structural parameter of the support layer (S_s). Hence the mass transfer coefficient in the support layer (k_s) can be calculated as Eq. (4).

$$k_s = \frac{D_s}{l_{eff}} = \frac{D_D \varepsilon}{l_{sl} \tau} = \frac{D_D}{S_s} \quad (4)$$

From the boundary condition in the support layer in Eq. (3), Eq. (5, 6) are obtained from integrating Eq. (1). Consequently, the solute concentration at the interface between the support and active layer (C_i) was defined as below:

$$C_i = \exp\left(-\frac{J_w}{k_s}\right)\left(C_{sl} + \frac{J_s}{J_w}\right) - \frac{J_s}{J_w} \quad (5)$$

$$C_i = C_{sl}\exp\left(-\frac{J_w}{k_s}\right) - \frac{J_s}{J_w}\left[1 - \exp\left(\frac{-J_w}{k_s}\right)\right] \quad (6)$$

where $C_{sl}\exp\left(-\frac{J_w}{k_s}\right)$ is the dilutive concentration of DS due to DS convection and $\frac{J_s}{J_w}\left[1 - \exp\left(\frac{-J_w}{k_s}\right)\right]$ is the loss of draw solute due to reverse solute diffusion (RSD). Past work has demonstrated that the ratio of reverse draw solute flux to the water flux (J_s/J_w) can be expressed as follows [35]:

$$\frac{J_s}{J_w} = \frac{B}{AnRT} \quad (7)$$

where A is the water permeability coefficient and B is the solute permeation coefficient, n is the number of dissolved species e.g., 2 for NaCl, R is the ideal gas constant, and T is operating temperature. This ratio is taken to be a constant coefficient [35].

2.2. External concentration polarization

The effect of ECP at the membrane surface needs to be considered when developing a model for the overall performance of the FO membrane [28] [36]. A further decrease in effective osmotic pressure is attributable to both concentrative feed solution (concentrative ECP) and dilutive draw solution (dilutive ECP). Using the same differential equation, and applying it to boundary layers on the draw and feed solutions, two additional equations are obtained.

For the draw side, the boundary condition at the interface between the support layer and the bulk draw solution is expressed below:

$$\begin{cases} x = 0, C = C_{D,b} \\ x = \delta_D, C = C_{sl} \end{cases} \quad (8)$$

where $C_{D,b}$ is the concentration of solute in the bulk draw solution, δ_D is the thickness of dilutive ECP in the draw side, and C_{sl} is the solute concentration on the membrane surface of the support

192 layer. As integrated the solute concentration on the membrane surface of the support layer can be
193 expressed in Eq. (9):

194 $$C_{sl} = C_{D,b}\exp\left(\frac{-J_w}{k_D}\right) - \frac{J_s}{J_w}\left[1 - \exp\left(\frac{-J_w}{k_D}\right)\right] \quad (9)$$

195 where $C_{D,b}\exp\left(-\frac{J_w}{k_D}\right)$ is the dilutive concentration of DS due to DS convection and
196 $\frac{J_s}{J_w}\left[1 - \exp\left(\frac{-J_w}{k_D}\right)\right]$ is the loss of draw solute due to reverse solute diffusion (RSD), and $\underline{k_D}$ is the
197 mass transfer coefficient on the draw side. It is dependent on the hydrodynamic condition on the
198 membrane surface.
199 Similarly for the feed side, the boundary condition at the interface between the cake layer and the
200 bulk feed solution is expressed below:

201 $$\begin{cases} x = 0, C = C_{F,b} \\ x = \delta_F, C = C_{F,c} \end{cases} \quad (10)$$

202 where $C_{F,b}$ is the concentration of solute in the bulk feed solution, δ_F is the thickness of the
203 concentrative ECP on the feed side, $C_{F,c}$ is the solute concentration on the surface of foulant
204 cake layer. Consequently, the solute concentration on the surface of the foulant cake layer ($C_{F,c}$)
205 can be expressed as Eq. (11):

206 $$C_{F,c} = C_{F,b}\exp\left(\frac{J_w}{k_F}\right) + \frac{J_s}{J_w}\left[\exp\left(\frac{J_w}{k_F}\right) - 1\right] \quad (11)$$

207 where $C_{F,b}\exp\left(\frac{J_w}{k_s}\right)$ is the concentration of FS due to FS convection and $\frac{J_s}{J_w}\left[\exp\left(\frac{J_w}{k_F}\right) - 1\right]$ is an
208 accumulation of draw solute due to reverse solute diffusion (RSD), and $\underline{k_F}$ is the mass transfer
209 coefficient on the feed side. This depends on the hydrodynamic condition at the membrane surface
210 on the feed side.
211 The local mass transfer for the hydrodynamic ECP boundary layer of fluids is related to a primary
212 local Sherwood number. In general terms, prediction on the local mass transfer coefficient on both
213 the feed side (k_F) and draw side (k_D) can be made from a well-known Graetz equation of
214 rectangular channel. However, our current channel is relatively short and the membranes surface
215 has a 'ridge and valley' structure typical of TFC membranes. Both of these affects will make

predictions from theory problematic and the Graetz equation is best used to check a directly calculated value.

Combining the equations above, and as reported elsewhere, the water flux in the absence of foulant can be expressed as [37]:

$$J_w = A\left\{\frac{\pi_{D,b}\exp\left[-J_w\left(\frac{1}{k_D}+\frac{S_S}{D_D}\right)\right]-\pi_{F,b}\exp\left(\frac{J_w}{k_F}\right)}{1+\frac{B}{J_w}\left\{\exp\left(\frac{J_w}{k_F}\right)-\exp\left[-J_w\left(\frac{1}{k_D}+\frac{S}{D_D}\right)\right]\right\}}\right\} \quad (12)$$

Therefore, we define the external mass transfer coefficients using four actual data sets of fluxes from baseline experiments with various DS and a foulant free FS. Based on A, B and S determined before, the methodology of obtaining the best estimates of mass transfer coefficients was to change the value of k_F and k_D until a sum of square error (SS_{err}) between measured flux and estimated flux achieve a minimum value. The method has been used previously elsewhere [38]. The outcome is summarized in Table 1.

As using different draw solution concentration (0.75, 1.5 M), it should be noted that change in external mass transfer coefficients need to be considered. As reported these values could be linked to the base values, expressed by Eq. 13 [38]:

$$\frac{k}{k_o} = \left(\frac{D}{D_0}\right)^{2/3} \quad (13)$$

2.3. Cake-enhanced concentration polarization

For a fouled membrane in a FO process it is has been recognized that the build-up of the foulant cake layer not only causes a hydraulic resistance but there is also hindered diffusion of solutes. As reported previously [33], the cake layer creates the porous and tortuous structure of foulant and one can define a cake structural parameter (S_c) consisting of the cake layer thickness (δ_c), tortuosity (τ_c), and porosity (ε_c), such that $S_c = \delta_c\tau_c/\varepsilon_c$. Boundary conditions were defined as:

$$\begin{cases} x = 0, C = C_{F,c} \\ x = S_c, C = C_{al} \end{cases} \quad (14)$$

Consequently, the draw solute concentration at the interface between the foulant cake layer and active layer surface can be expressed by Eq. (15).

$$C_{al} = C_{F,c} \exp\left(\frac{J_w S_c}{D_c}\right) + \frac{J_s}{J_w}\left[\exp\left(\frac{J_w S_c}{D_c}\right) - 1\right] \quad (15)$$

where D_c is the diffusion coefficient of solutes in the foulant cake layer. The term D_c/S_c represents the mass transfer k_c within the foulant cake layer.

2.4. Modeled water flux of a fouled membrane

Based on the solution-diffusion model for the nonporous rejection layer, water flux is defined as follows:

$$J_w = A\,\Delta\pi_m \quad (16)$$

where A is the water permeability coefficient, and $\Delta\pi_m$ is the effective osmotic pressure. However, the pressure drop induced by the foulant cake layer decreases the effective driving force [33] [39]. The pressure drop across the cake layer (ΔP_c) can be expressed as a function of cake structural parameter (S_c) and pore hydraulic diameter of the cake layer (D_h). Thus,

$$\Delta P_c = \frac{32\mu S_c J_w}{D_h^2} \quad (17)$$

Therefore, water flux across the active layer should be calculated from:

$$J_w = A\,(\Delta\pi_m - \Delta P_c) = A\,(\Delta\pi_m - \frac{32\mu S_c J_w}{D_h^2}) \quad (18)$$

where D_h is the hydraulic diameter of the pores in the cake and μ is the viscosity of the solution within the cake layer.

Combining Eq. (6) with Eq. (9), C_i can be expressed as follows:

$$C_i = C_{D,b} \exp\left[-J_w\left(\frac{1}{k_D} + \frac{S_s}{D_d}\right)\right] + \frac{J_s}{J_w}\left\{\exp\left[-J_w\left(\frac{1}{k_D} + \frac{S_s}{D_D}\right)\right] - 1\right\} \quad (19)$$

Combining Eq. (11) with Eq. (15), C_{al} can be expressed as follows:

$$C_{al} = C_{F,b}\, exp\left[J_w\left(\frac{1}{k_F} + \frac{S_c}{D_c}\right)\right] + \frac{J_s}{J_w}\left\{exp\left[J_w\left(\frac{1}{k_F} + \frac{S_c}{D_c}\right)\right] - 1\right\} \quad (20)$$

From Eq. (19) from Eq. (20), the effective concentration difference ($\Delta C_m = C_i - C_{al}$) can be obtained as follows:

$$\Delta C_m = \frac{C_{D,b}\, exp\left[-J_w\left(\frac{1}{k_D}+\frac{S_S}{D_D}\right)\right]-C_{F,b}\, exp\left(\frac{J_w}{k_F}+\frac{\boldsymbol{S_C}}{\boldsymbol{D_C}}\right)}{1+\frac{B}{J_w}\left\{\exp\left(\frac{J_w}{k_F}+\frac{\boldsymbol{S_C}}{\boldsymbol{D_C}}\right)-\exp\left[-J_W\left(\frac{1}{k_D}+\frac{S_S}{D_D}\right)\right]\right\}} \quad (21)$$

Assuming osmotic pressure is linearly proportion to the salt concentration, then from Eq. (21) and Eq. (18) the modeled water flux of a fouled FO membrane can be calculated using Eq. (22)

$$J_w = A(\Delta\pi_m - \Delta P_c) = A\left\{\frac{\pi_{D,b}\exp\left[-J_w\left(\frac{1}{k_D}+\frac{S_S}{D_D}\right)\right]-\pi_{F,b}\exp\left(\frac{J_w}{k_F}+\frac{\boldsymbol{S_C}}{\boldsymbol{D_C}}\right)}{1+\frac{B}{J_w}\left\{\exp\left(\frac{J_w}{k_F}+\frac{\boldsymbol{S_C}}{\boldsymbol{D_C}}\right)-\exp\left[-J_W\left(\frac{1}{k_D}+\frac{S_S}{D_D}\right)\right]\right\}}-\frac{32\mu S_C J_w}{D_h^2}\right\} \quad (22)$$

3. Materials and methods

3.1. FO membrane and laboratory-scale system

The FO membrane used in the current study, was a polyamide-thin film composite (PA-TFC) cut from a spiral wound FO element (CSM FO-8040, Toray), followed by soaking in deionized (DI) water and then stored at 4 °C. Thickness, morphology, hydrophobicity/hydrophilicity, surface roughness of the pristine membrane was measured. Such intrinsic properties of the TFC membrane i.e., water permeability (A), solute permeability (B), and structural parameter (S) were simultaneously determined using the non-pressurized method with single-stage FO based test. This method has been fully described previously [40]. The specific properties of the membrane are presented in Table S-1.

As illustrated in Fig. S1, the FO cell made of acrylic consisted of two rectangular channels with dimensions of 75 mm (length) × 25 mm (width) × 3 mm (height) and an effective membrane area of 1875 mm^2. No spacer was used for either the feed or draw channels of the FO cell. An identical flow rate of 300 mL/min (equivalent cross-flow velocity (CFV) of 6.66 cm/s) was maintained in both the feed and draw channels. Operation in counter-current mode was set using the magnetic drive gear pumps. Digital pressure gauges with a precision of 0.005 bar were installed in the DS and FS channels to monitor the maintenance of FO mode. For both the feed solution (FS) and draw solution (DS), the temperature was maintained at 24±1 ^oC using a water bath. For all experiments, the FO system was operated with an active layer facing the feed solution (AL-FS). An electronic

mass balance was used to record the variation in the DS mass and then converted to volume to determine the water flux as Eq. 23.

$$J_w = \frac{1}{A_m}\frac{\Delta V}{\Delta t} \quad (23)$$

where J_w is the water flux (LMH) at time t, A_m is the effective membrane area (0.001875 m^2 in the current study), V is the volume of collected permeate (L), and t is the time for collecting the permeate (h).

Meanwhile, a conductivity meter was installed into the feed tank to measure the solute mass diffused from draw solution to feed solution. Reverse solute flux (RSF) was calculated as Eq. (24)

$$J_s = \frac{C_{F,f}\left(V_{F,0} - J_w A_m t\right) - C_{F,0}V_{F,0}}{A_m t} \quad (24)$$

where $V_{F,f}$ is the final volume of the feed solution, $V_{F,0}$ is the initial volume of the feed solution, $C_{F,f}$ in the final concentration of the feed solution, and $C_{F,0}$ is the initial concentration of the feed solution.

3.2. Organic foulants

Alginate (ALG), Bovine serum albumin (BSA), Humic acid (HA) were used as adequate models of organic matters to represent for polysaccharides, protein, and humic matter, which are major foulants in wastewater (WW) [41] [42]. They were supplied in powder form (Sigma-Aldrich, USA). The HA stock solution (2 g/L) was prepared by dissolving the powder into 0.01 mol/L NaOH solution (pH> 12) to ensure complete dissolution, followed by filtering through a 1 µm glass fiber membrane to remove residual non-dissolved matter. Meanwhile, the other stock solutions were prepared by dissolving 2 g of the powder in 1 L of DI water. All solutions were stirred over 24 h and then stored at 4^0C.

3.3. Fouling experiments

Feed solution for the baseline and fouling tests had a consistent concentration of 10 mM NaCl to avoid changes in ionic strength (IS), causing unintended changes in flux behavior. To simulate real WW the desired foulant concentration was set at 160 mg/L based on findings from a previous

study [43]. As denoted in Table 1, fouling was investigated under two scenarios: low protein fraction (ALG: HA: BSA of 2:2:1 wt/wt) and high protein fraction (ALG: HA: BSA of 2:1:2 wt/wt). An estimate of a critical flux value was made based upon our previous study [23] and initial fluxes around this value were selected for investigation; values were 24, 30, and 34 LMH (corresponding to DS concentration of 0.75; 1.0; 1.5 M NaCl, respectively). A long-term operation was run over 12 cycles giving 120 h operation in total. To minimize the increase in foulant concentration in FS, after a cycle of 10 hours fresh FS and DS were prepared for the next cycle. For the former fouling scenario, the flux decline patterns were observed under different fluxes. In addition, the effect of feed compositions (low/high protein fraction present in WW) on the fouling reversibility was also evaluated during operation. In detail, for all FO fouling tests a membrane coupon was placed in the test cell and the flow rate of the DS and FS adjusted to achieve the desired CFV value of 6.66 cm/s. Both solutions were prepared with the same volume of 2 L. A stabilization testing for 30 mins was performed using DI water for both the FS and DS sides prior to all experiments. A typical test included the baseline stage followed by the fouling one. A difference between the two stages was indicative of fouling by the foulants in the FS. The flux decline curve in the baseline test was used to normalize the flux decline curves in the fouling test, thereby obtaining a measure of the flux decline due to fouling alone. This normalization has been described in detail elsewhere [17].

Table 1. Feed solution composition

Feed solution	Foulant concentration (mg/L)	Ionic strength (mM)
Baseline test	-	10
Fouling test with Simulated wastewater		
ALG: HA: BSA (2:2:1 wt/wt) (low protein fraction)	160	10
ALG: HA: BSA (2:1:2 wt/wt) (high protein fraction)	160	

Examination of fouling reversibility and membrane autopsies were performed. For calculating fouling reversibility (FR), physical flushing on the feed side using DI water was immediately

performed for 15 mins with an increased CFV value of 13.32 cm/s, followed by a measurement of flux at the initial CFV. In addition, when flux declines by over 15%, chemical cleaning was adopted to recover flux. The conditions for chemical cleaning were 1% NaOH, at a feed flow rate of 600 mL/min (CFV of 13.32 cm/s), cleaning time for 15 mins, followed by DI flushing for 15 mins to remove residual NaOH. Flux recovery or fouling reversibility (FR) in FO was calculated as follows [21].

$$FR\ (\%) = \frac{J_{xr} - J_{xf}}{J_{xi} - J_{xf}} \times 100 \quad (25)$$

where J_{xi} is the water flux of a virgin membrane, J_{xf} is water flux after fouling (LMH), and J_{xr} is the water flux after physical or chemical cleaning (LMH).

3.4. Quantification of CPs and the cake foulant-enhanced CP

Based on theory, the loss of driving force is attributed to the effects of ICP in the support layer, ECPs (concentrative ECP in the feed side, and dilutive ECP on the draw side) and additional cake layer-ECP phenomena. These effects can be quantified by Eq. (26), Eq. (27), Eq. (28), and Eq. (29) respectively:

$$Dilutive\ ICP\ = \frac{C_{sl} - C_i}{C_{D,b} - C_{F,b}} \times 100 \quad (26)$$

$$Dilutive\ ECP = \frac{C_{D,b} - C_{sl}}{C_{D,b} - C_{F,b}} \times 100 \quad (27)$$

$$Concentrative\ ECP = \frac{C_{F,c} - C_{F,b}}{C_{D,b} - C_{F,b}} \times 100 \quad (28)$$

$$Cake\ 'foulant\ enhanced'\ CP\ = \frac{C_{al} - C_{F,c}}{C_{D,b} - C_{F,b}} \times 100 \quad (29)$$

3.5. Cake structural parameter and fouling resistance determination

Cake structural parameter (S_c) of the foulant layer obtained from the conditions of different fluxes, various feed compositions were calculated for comparison. In detail, the cake structural parameter is predicted in an iterative process by minimizing the error between calculated flux ($J_{w,\ cal}$) and experimental flux ($J_{w,\ measured}$). Operating conditions (Table 2) and model parameters (Table 3)

were used to calculate the cake structural parameter. A detailed calculation procedure is shown in Fig. 2.

Table 2. Operating conditions of membrane channel

Condition	Description	Unit	Value
L	Length of membrane channel	m	0.075
W	Width of membrane channel	m	0.025
d	Height of membrane channel	m	0.003
T	Temperature	K	293
CFV	Cross-flow velocity (Both feed and draw sides)	m/s	0.067

Table 3. Model parameters used for calculating cake structural parameter

Parameter	Description	Unit	Value
A	Water permeability coefficient	$m^3/m^2.s.Pa$	$9.14x10^{-12}$ (This study)
		LMH Bar^{-1}	3.29 (This study)
B	Solute permeability coefficient	$m^3/m^2.s$	$4.75x10^{-7}$ (This study)
		LMH	1.71 (This study)
S_s	Structural parameter of the support layer	m	$2.10x10^{-4}$ (This study)
D_D	Bulk diffusion coefficient of draw solution	m^2/s	$1.38x10^{-9}$ (1.5 M NaCl) [44]
			$1.41x10^{-9}$ (1.0 M NaCl) [44]
			$1.43x10^{-9}$ (0.75 M NaCl) [44]
D_F	Bulk diffusion coefficient of feed solution	m^2/s	$1.62x10^{-9}$ [44]
D_C	Diffusion coefficient in foulant cake layer	m^2/s	$1.29x10^{-9}$ [33]
μ	Dynamic viscosity of water	kg/m.s	$8.9x10^{-4}$
ρ	Density of water	kg/m^3	998
D_h	The hydraulic pore diameter of foulants	m	$2.58x10^{-7}$ (This study)

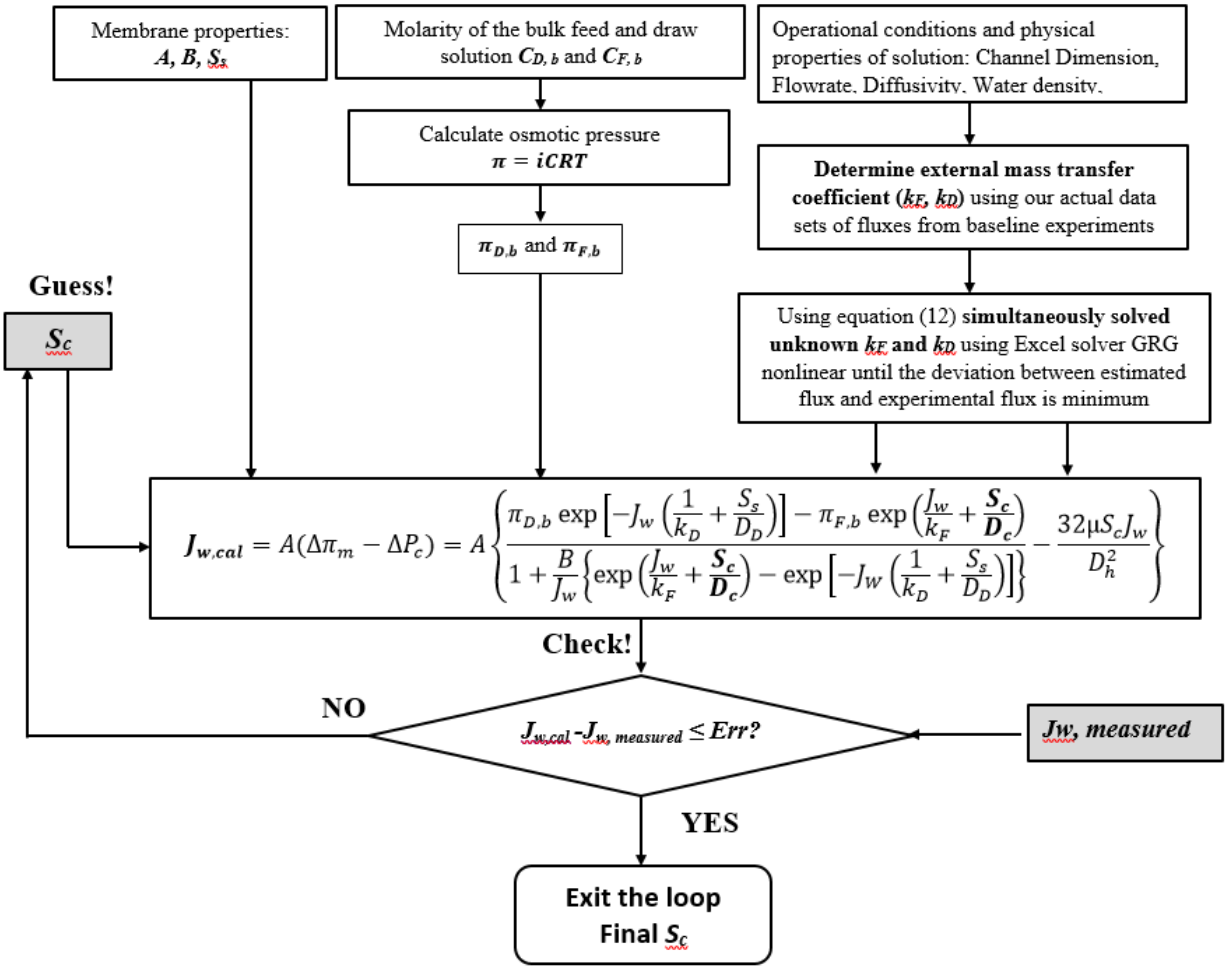

Figure 2. Flow chart of the calculation procedure of cake structural parameter (S_c)

Membrane resistance (R_m) and resistance due purely to concentration polarization (R_{cp}) were determined using Eq. (33), which was derived based on the osmotic-resistance for osmotically driven membrane process [45]:

$$J_w = \frac{Driving\ force}{\mu(R_m+R_{cp})} \quad (33)$$

When fouling occurs, total resistance (R_t) will impact water flux and is calculated in Eq. (34). This resistance includes membrane resistance (R_m), fouling resistance (R_f), and resistance due purely to concentration polarization (R_{cp})

$$R_t = \frac{Driving\ force}{\mu J_{W,f}} \quad (34)$$

And the foulant resistance R_f is then calculated by subtracting the total resistance R_t with the pristine membrane resistance R_m and resistance of concentration polarization R_{cp} as follow:

$$R_f = R_t - R_m - R_{cp} \quad (35)$$

3.6. Foulant characterization

The morphology (surface and thickness) and composition (e.g., functional groups) of the fouling layer were characterized by Field Emission Scanning Electron Microscopes (FE-SEM) and the Attenuated Total Reflectance-Fourier Transform Infrared Spectroscopy (ATR-FTIR), respectively. In detail, surface and cross-sectional images of morphological features (virgin, fouled, and cleaned FO membranes) were observed using a Field Emission Scanning Electron Microscopes (FE-SEM) (S-4700, Hitachi, Japan) to examine the presence and the morphology of foulant on the membrane surface. Prior to SEM analysis, all samples were air-dried in a desiccator overnight and subsequently coated with platinum for 3 min. Spectra of samples were obtained using Attenuated Total Refractive-Fourier Transform Infrared (ATR-FTIR) Spectroscopy (Perkin-Elmer IR 2000 Series, Billerica, MA, USA) with a resolution of 4 cm^{-1} in the range of 4000 cm^{-1} to 700 cm^{-1}. These measurements were used to indicate the organic functional groups of the pristine, fouled, and cleaned membrane. All samples were air-dried in a desiccator overnight before analysis. The aggregation size of foulants was measured by dynamic light scattering.

4. Results and discussion

4.1. Flux decline patterns and the fouling reversibility under operating conditions

Based on a critical value for complex fouling (30 LMH) obtained from our past work [23], a long-term 120 h investigation into different fluxes, at and either side of 30 LMH, was carried out. The water flux was normalized to indicate the extent of fouling. As denoted in Fig. 3a, for the condition of 34 LMH a flux declined of 15% was observed in a 10 h operation after which there was a physical clean. This trend was maintained for the first six cycles, i.e. 60 h operation. As observed in Fig. S3-a1, b1, a cake layer with a thickness of 4.78 ± 0.32 μm was formed on the membrane surface. This layer made up an increased portion of total resistance and caused cake-ECP; thus this was the cause of the significant flux decline. As fouling became severe, physical cleaning was conducted to recovery the initial flux but it could only attain low fouling reversibility; FR was 82-

85% during 60 h operation. This can be attributed to the fact that operation was above the critical value previously identified [16] [23]. During the first 50 h, the FR decreased from 85% to 79%. Due to foulant accumulation on the membrane surface higher decreases in water flux were observed in subsequent cycles. Direct observations indicated that foulants still remained on the membrane surface after imposing physical cleaning (Fig S3-c1, d1). Under this relatively high flux (34 LMH) the fouling layer becomes denser and thicker with time (Fig S3-a1, b1, and a2, b2) which renders the fouling layer less sensitive to changes in hydrodynamic conditions i.e., increasing CFV. The result is irreversible fouling. To recover the membrane a chemical cleaning was conducted after 70 h. As expected the water flux was fully restored (100% FR). However, this action not only increased the initial flux to 37 LMH but also altered the flux decline pattern which became more severe; there was a decrease of 27% after each subsequent 10 h operation. This implies that the PA-TFC membrane surface could be modified by chemical agents, which resulted in a change in water flux behavior. As reported, chemical cleaning agents caused changes in membrane properties [46]. The pore size of TFC could be enlarged after alkaline exposure and this is attributed to the increased electrostatic interactions among the deprotonated carboxylic functional groups of the polyamide active skin layer [47]. Since the FR continued to reduce from 93% to 88% after 100 h of operation, a second chemical cleaning was made. At 27% the subsequent flux decline remained the same.

To minimize the degree of fouling the study turned to lower fluxes and the frequency of physical cleanings was reduced as shown in Fig. 3. For 30 LMH a flux decline of 12% was observed over 20 h operation. For 25 LMH the decline was 3% over 40 h operation, indicating very minor fouling. This condition appeared below critical values, which facilitated a sustainable operation and cleaning minimization [48]. It is important to note that for both 30 and 25 LMH water flux was restored fully by a physical cleaning. To further elucidate the different flux decline patterns, the influence of CPs (ECPs, ICP, and Cake-ECP) and the fouling resistance were determined. The results for the different fluxes are presented later in section 4.3.

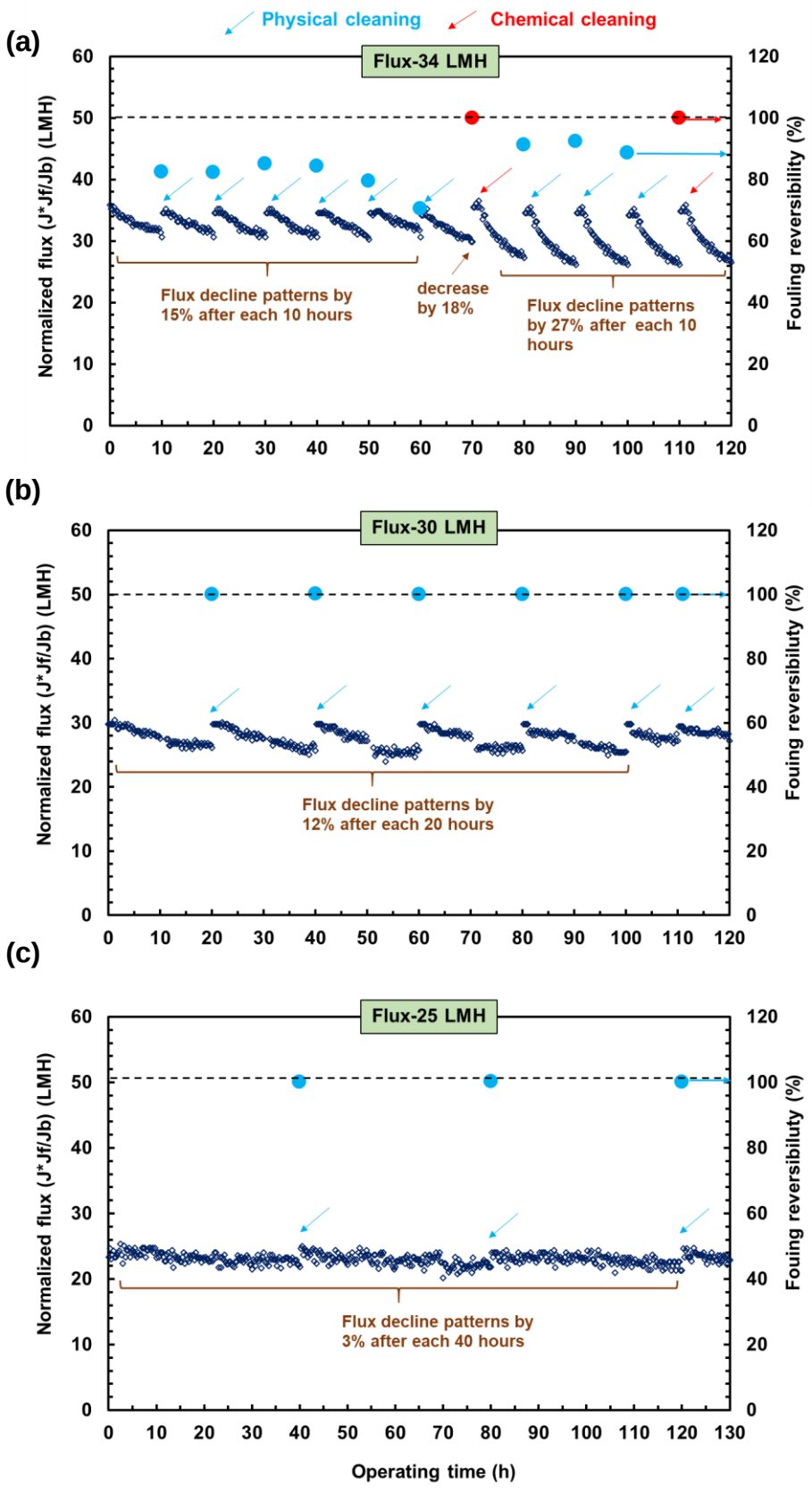

Figure 3. Flux decline patterns and the fouling reversibility under different fluxes: (a) 34 LMH; (b) 30 LMH and (c) 25 LMH. All experiments were conducted at the long-term operation of 120-130 h. J_o *x* J_f/J_b is a normalized representation of the extent of membrane fouling. J_o represents the

441 initial flux, J_f is the flux in the fouling test, J_b is the flux in the baseline flux. Simulated wastewater
442 consists of complex foulants of ALG, HA, and BSA (ALG: HA: BSA= 2:2:1 wt/wt e.g., low
443 protein fraction) and the foulant concentration of 160 mg/L.
444 An analysis of the influence of flux upon FR and flux decline is shown in Fig. 4. As severe fouling
445 occurred at a flux of 34 LMH, the flux declines of 13%; 25% and 32% were observed in 10 h, 20
446 h and 40 h operation. The corresponding fouling layer thicknesses were 4.78 ± 0.32 µm, 10.96 ±
447 0.82 µm, 20.05 ± 0.52 µm respectively (Fig S3- b1, b2, b3). It is generally accepted that a lower
448 % flux decline facilitated higher FR. Although the same flux decline was roughly 12% after 10h
449 and 20 h operation observed for 30 and 34 LMH fluxes, respectively, the former (FR 100%)
450 exhibited a higher FR than the latter (FR 82%). Furthermore full restoration was achieved at 30
451 LMH using simple physical cleaning. This value corresponds with the critical value determined in
452 our past works [16] [23].
453 For the case of 34 LMH, as the extent of FR via physical cleaning decreased from 82% to 73% the
454 degree of flux decline increased from 13 to 21%. Interestingly, there was no significant difference
455 in FRs once physical cleaning was implemented after 20 h (FR 74%) and 40 h (FR 73%), as shown
456 in Figure 4. After cleaning visualization of the outcomes was made by SEM images indicated that
457 a comparable thickness of cake layer i.e., 0.82 ± 0.07 µm and 0.91 ± 0.15 µm were for the cases
458 of 20 h and 40 h operation, respectively (Fig S3-d2, d3). This suggests that for fouling by WW
459 possessing a low protein fraction, the upper cake layer could be readily removed using simple
460 physical cleaning and that the core underlying layer changes slowly.
461 In the literature, the fraction of polysaccharide, protein, and humic acid in WW depends on the
462 treatment stage and technology [41]. Therefore it was of interest to investigate the effect of feed
463 compositions (low protein and high protein fractions) on the FO performance see next section.

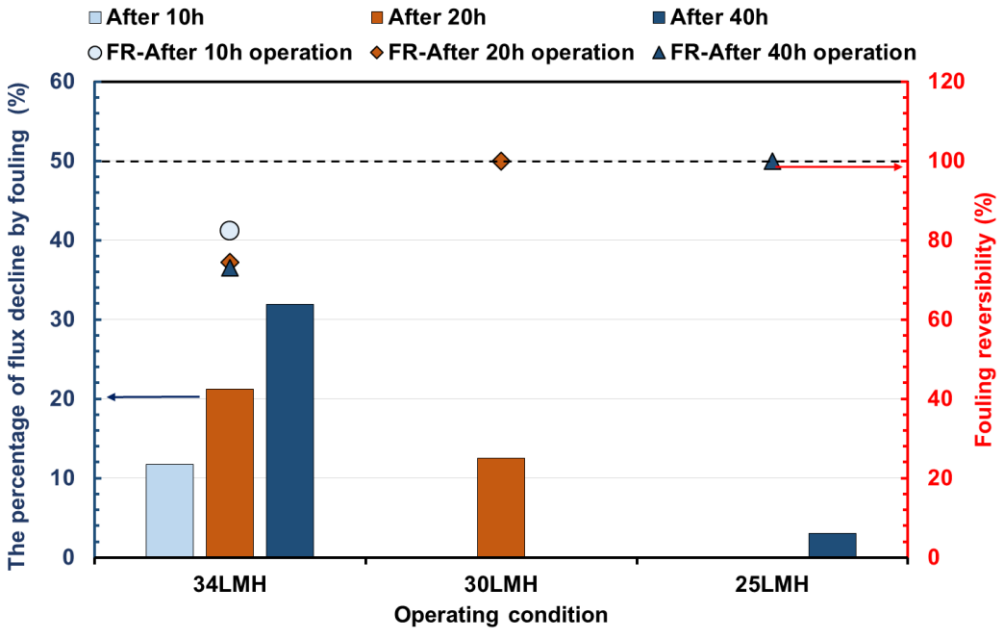

464

465 **Figure 4.** Comparison of the extent of flux decline and fouling reversibility (FR) under different
466 fluxes (34; 30; 25 LMH). A physical cleaning was conducted for scenarios: after 10 h, 20 h, or 40
467 h depending on the initial flux. Condition of physical cleaning: DI water at CFV of 13.2 cm/s for
468 15 mins.

469

470 **4.2. Effect of feed compositions on % flux decline and the fouling reversibility**

471 To investigate the influence of the level of the protein fractions present in WW, a flux of 30 LMH
472 was chosen and the % flux decline and FR were assessed over 100 h operation (Fig. 5-a). For both
473 levels of protein, the flux decline gradually increased, possibly towards a plateau. This is attributed
474 to a build-up of irreversible fouling. For just the initial stage of 20 h, the extent of flux decline was
475 comparable for the two levels of protein, with an average decline of around 12%. This was
476 confirmed by surface and cross-sectional analyses of the fouled membrane (Fig. 5-b, c, d); after
477 operated in 20 h the cake layer thicknesses were 2.51 ± 0.25 µm and 2.90 ± 0.20 µm for the high
478 and low protein cases, respectively. Thereafter, the fouling extent became more serious for the
479 high level of protein, with flux decline reaching 18% after 100 h operation, compared with 14%
480 for the lower level of protein. These results can probably be attributed to different cleaning-
481 efficiency from two scenarios. Whilst the water flux was fully restored (FR 100%) for WW

possessing low protein fouling, this was not expected for high protein fouling in which the FR was low (67%) after 100 h operation. This fact was confirmed through measuring the cake layer thicknesses after cleaning. As shown in Fig. 5-d, g, values of 0.46 ± 0.05 µm were found for low protein fraction compared with 1.39 ± 0.20 µm for high protein fraction. It is noted that the reverse solute flux of the fouled membrane i.e., 7.4-9.5 $g/m^2.h$ was lower than that of the pristine membrane i.e., 11.9 $g/m^2.h$ (Fig. 6-a). This indicates that the reverse solute flux decreased with the development of the cake layer.

As previously reported the formation of complex organic fouling layer rendered the membrane more negatively charged [5] [23]. This increase could reduce the transport of draw solution ions in the reverse direction. Likely, the reverse solute flux of Cl^- ion was hampered by an enhanced electrostatic interaction with the more negatively organic fouling layer. As a final point on the RSF, it is noted that membrane fouled by low protein fraction yielded a higher RSF than that by high protein fraction and this can be probably attributed to different foulant structures e.g., cake structural parameter. Detailed calculation on this parameter is covered in section 4.3.2.

The FTIR analyses of the pristine membrane, the fouled membrane, and a cleaned membrane are presented in Fig. 6-b, c. These results indicated that the PA-TFC membrane comprised of a polysulfone layer and polyamide layer. Operation at either low or high protein conditions led to the formation of a cake layer on the membrane surface. Consequently, the peaks of the active layer and support layer of the pristine membrane were attenuated. The results for the fouled membranes, show the emergence of peaks. For the case of low protein fraction, peaks associated with quinone and ketone C-O bond, or aromatic rings (C=C) were found indicating the presence of HA in the top layer of the cake layer. For the high protein fraction the existence of protein –like substance was found. The results showed peaks such as amide A (N-H stretching), amide I (C=O stretching), amide II (N-H in-plane), amide III (C-N stretching), and CH_2 bending at 3280, 1643, 1532, and 1450, 1392 cm^{-1}, respectively. Since membrane fouled by low protein fraction could be restored readily, the FTIR spectra obtained from the cleaned membrane are likely to be similar to the

pristine membrane. Although a physical cleaning was implemented for membrane fouled by high protein fraction, the results of FTIR showed the presence of a protein-like substance on the cleaned membrane. Overall the findings indicate that protein is a persistent foulant and less sensitive to physical cleaning.

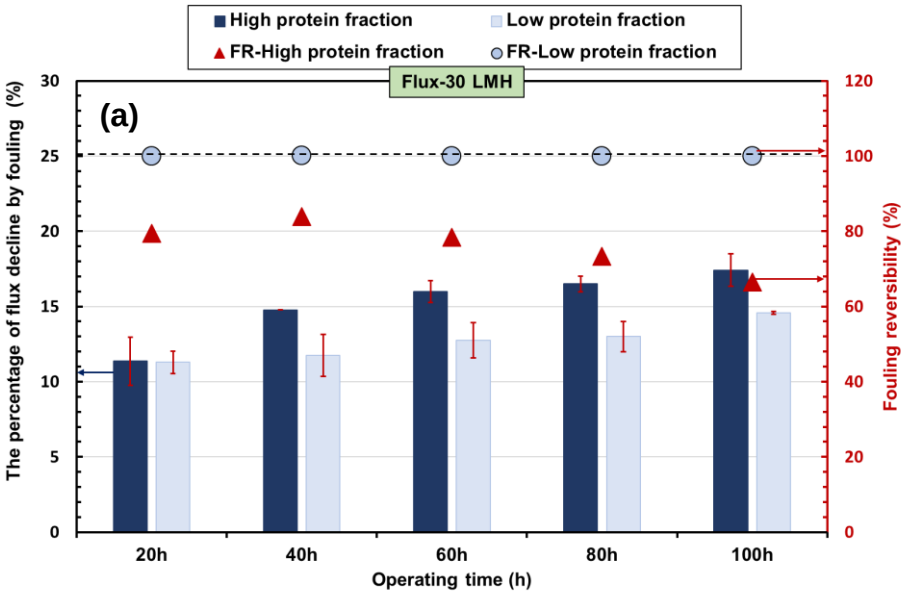

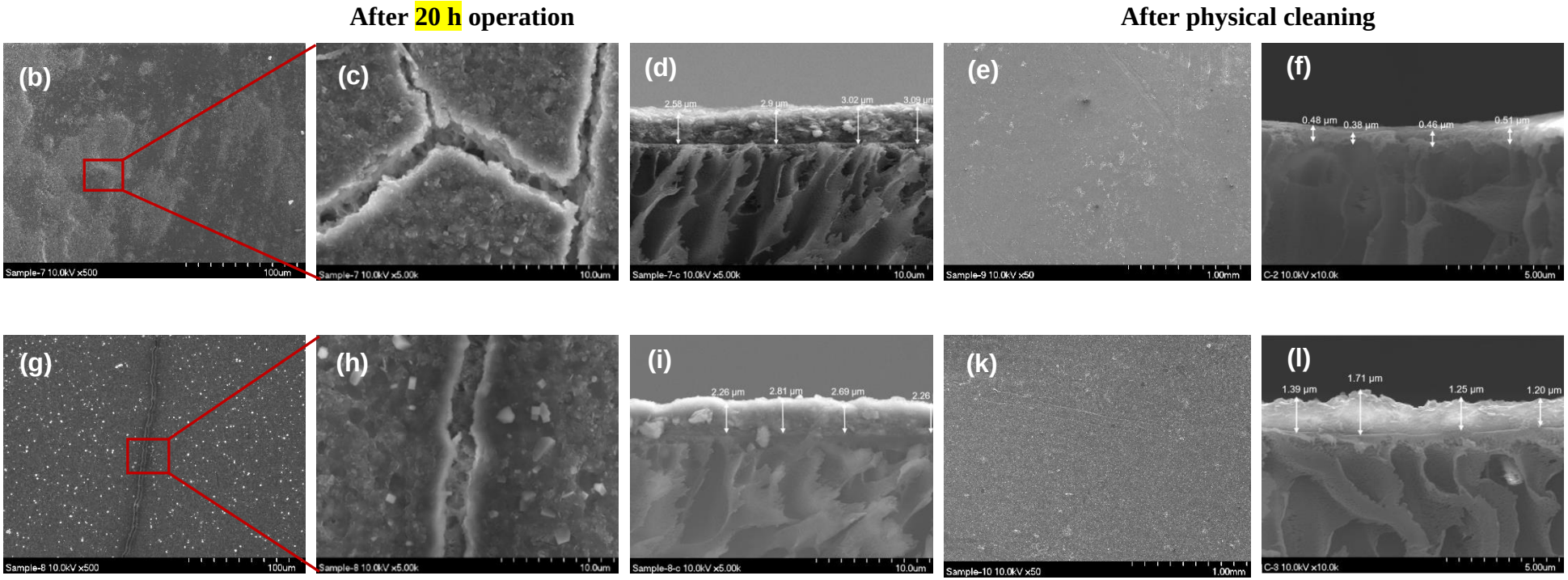

Figure 5. Comparison of % flux decline and the fouling reversibility under various feed compositions: low protein fraction (ALG: HA: BSA=2:2:1 wt/wt) and high protein fraction (ALG: HA: BSA=2:1:2 wt/wt) (a). All experiments had same flux of 30 LMH. A physical cleaning was conducted after each 20 h operation to define the fouling reversibility. Typical condition of physical cleaning: DI water with CFV of 13.2 cm/s for 15 minutes. SEM observation was conducted after 20 h fouling operation and after physical cleaning: low protein fraction (b, c, d, e, f) and high protein fraction (g, h, i, k, l)

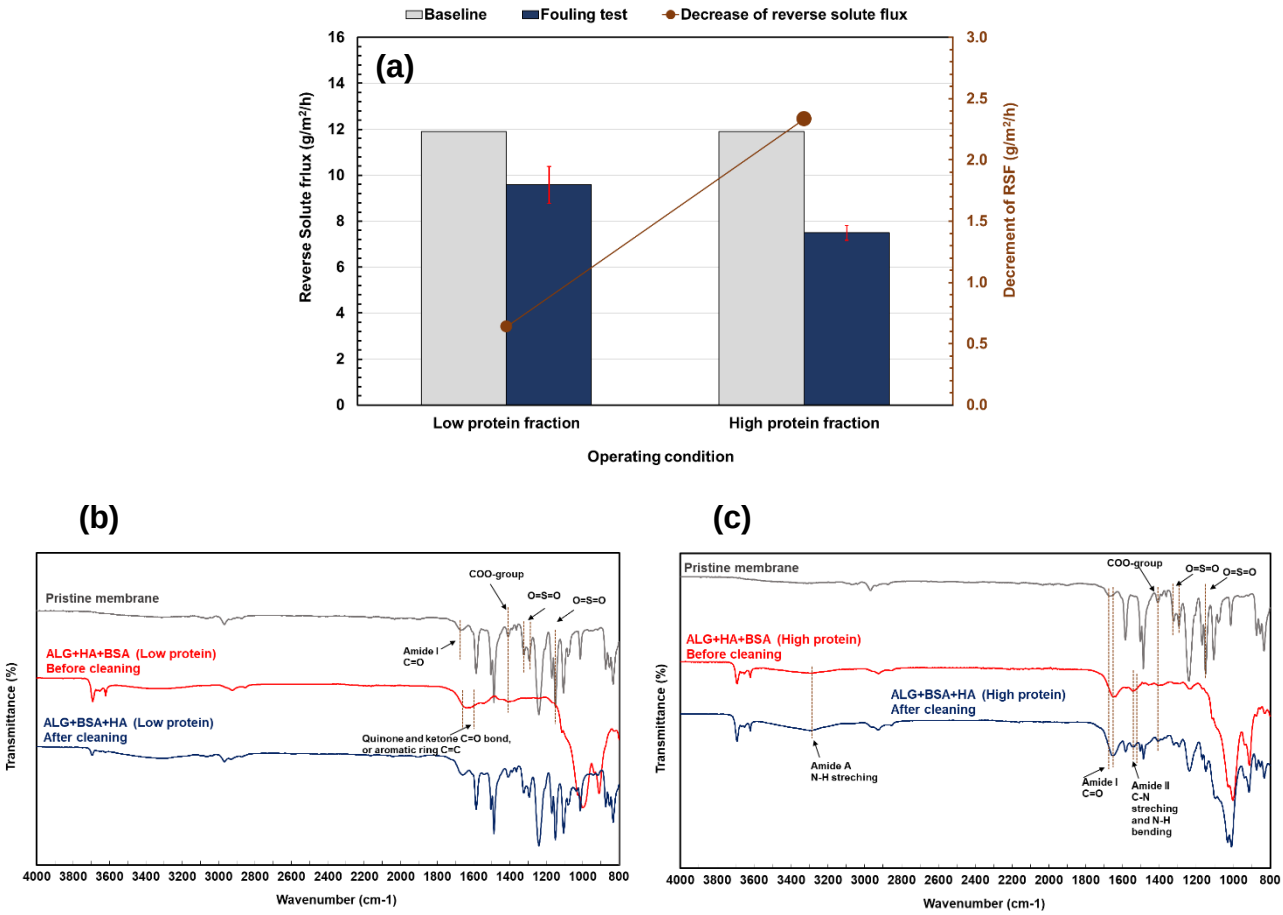

Figure 6. Comparison of reverse solute flux and FTIR measurements as operated at various feed compositions: (low protein of ALG: HA: BSA=2:2:1 wt/wt and high protein fraction of ALG: HA: BSA=2:1:2 wt/wt). All experiments were operated under the same flux of 30 LMH and foulant concentration of 160 mg/L. A reverse solute flux of pristine membrane (baseline) and fouled membrane (fouling test) after 100 h operation (a). FTIR measurements of the pristine membrane, fouled membrane, and cleaned membrane for the cases: low protein fraction (b) and high protein fraction (c).

4.3. Quantitative analysis of concentration polarization and fouling resistance

4.3.1. Different initial fluxes

In the FO membrane process, changes in water flux are the result not only of fouling but are also the result of consequential changes in CPs effects. Therefore, to obtain an insightful understanding

of the CPs and fouling effects, we quantified the extent of CPs in each of the transport layers, the fouling resistance of the foulant layer, for operation under different fluxes (Fig. 7).

It is generally accepted that higher overall driving force is attained at higher DS concentration and thus exhibits higher initial flux. Such initial effective driving forces were 8.24, 8.95 and 10.31 bar for operational fluxes of 25, 30, and 34 LMH, respectively (Fig. 7-a1, a2, b1 and b2). Whilst the effect of concentrative ECP in FS was very minor due to the low salt concentration (10mM NaCl), the dilutive ECP in DS and ICP had profound effects on the FO performance. These CP effects contributed 76.0%, 80.8%, and 85.3% on overall driving force under fluxes of 25, 30, and 34 LMH respectively (Fig S-5, 6, 7). After 20h operation the water flux declined by fouling was 12% and 25% for the fluxes of 30 and 34 LMH respectively and this is attributed to both decrease of the effective driving force (Fig. 7-a1, b-1) and increase in the fouling resistance (Fig. 7-c1, d1). As denoted in Fig. 7a-1, b-1, the cake layer-enhanced CP gradually increased in 20h operation and thus partially contributed to a decrease of the effective driving force. Operation at 30 LMH caused a relatively moderate decrease of the effective driving force from 8.95 to 5.45 bar whereas at a higher flux (34 LMH) it more that halved. As the cake layer evolved and flux reduced, the ICP effect diminished during the 20 h fouling test for both fluxes, and this is phenomenon has been labelled ICP-compensation [49]. As indicated by the results from SEM observation (Fig S4-b1, d1), after 20 h operation, the foulant layer thicknesses were 10.96 ± 0.82 μm and 2.90 ± 0.20 for 34 and 30 LMH respectively. Different thicknesses resulted in different fouling resistances and cake structural parameters. The corresponding values for 34 LMH were 3.37×10^{13} m^{-1} and 279 μm, which are higher than those for 30 LMH which were 2.88×10^{13} m^{-1} and 213 μm). Overall the results indicated that the flux chosen plays a pivotal role in fouling control.

572

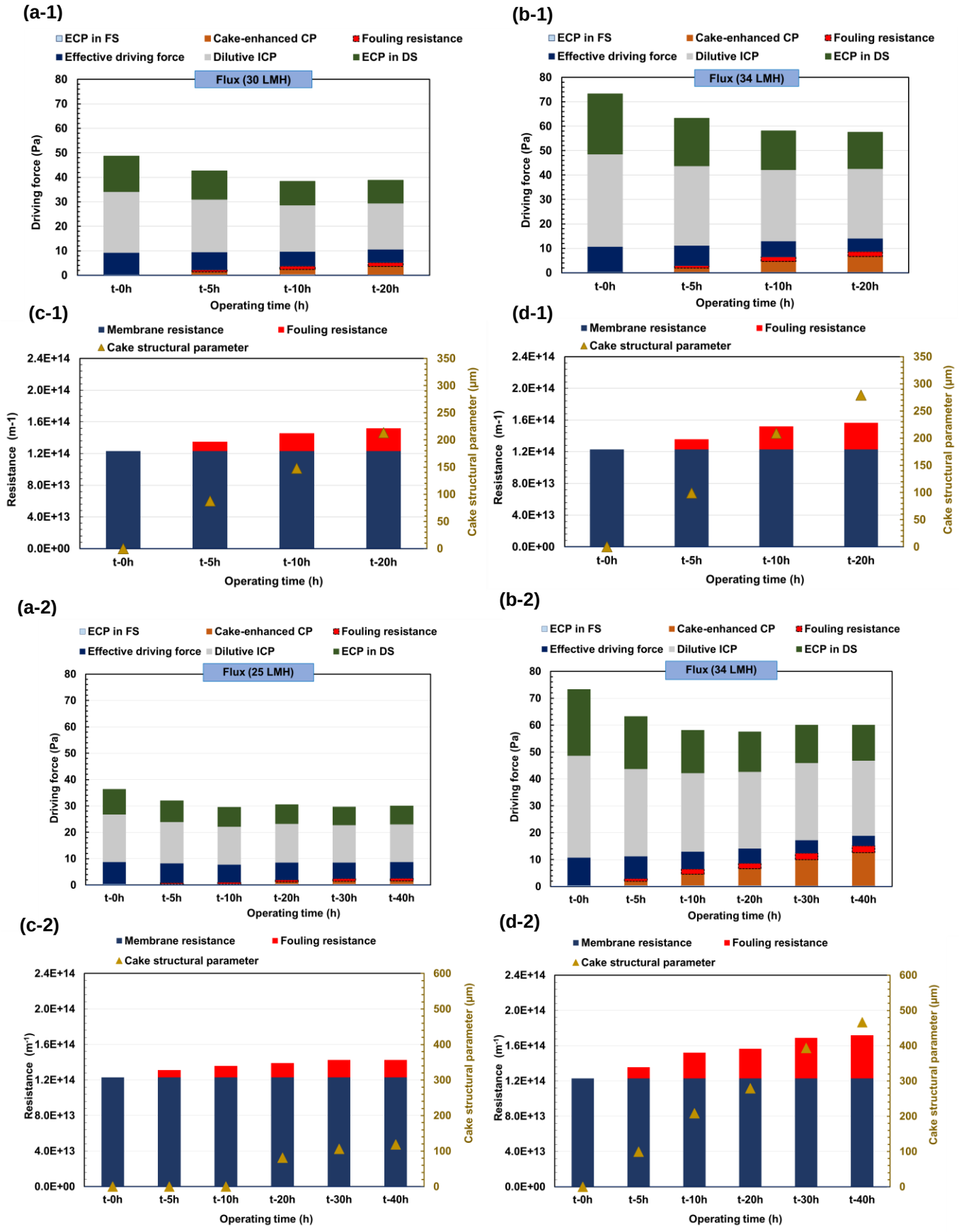

573

574

575 **Figure 7.** Change of CPs profile, cake structural parameter and fouling resistance with time under

576 different fluxes: 30 LMH (a-1, c-1) vs 34 LMH (b-1, d-1) for a 20 h fouling test conducted without

physical cleaning; 25 LMH (a-2, c-2) vs 34 LMH (b-2, d-2) for a 40 h fouling test conducted without physical cleaning.

As discussed in section 4.1, negligible fouling i.e., 3% flux decline in 40 h operation, was noticed for operation at 25 LMH, which is below the critical value. For 25 LMH the fouling resistance increased only marginally in 40 h operation (Fig. 7-c2), indicated that the impact of the cake layer on permeate is insignificant and this is due to a thin fouling layer (1.08 ± 0.23 µm) formed on the membrane surface. After 40 h operation, a minor influence of cake layer-enhanced CP and fouling resistance, respectively being 4.1% and 3.4% of the overall driving force (Fig S6-d), was observed. The cake had a small structural parameter (119 µm). By way of contrast, a negative impact was apparent at a high flux of 34 LMH where the flux decline led to significant decreases in the effective driving force. Compared to 25 LMH, a thicker cake layer of 20.05 ± 0.52 µm (Fig S4-b2) formed on the membrane surface resulting in a 2.5 times increase in the fouling resistance (4.88×10^{13} m^{-1}) and a four-fold increase in the cake structural parameter (466 µm). The cake layer not only posed an additional resistance to water transport but also enhanced solute concentration near the membrane surface; thereby reducing further the water flux. Although the ICP was offset by the cake layer-induced flux decline, the cake layer-enhanced CP was noticeable with it consuming 20.4% of the total driving force after 40 h operation (Fig S-6c). These findings quantify the significance of the cake layer-enhanced CP under high flux operation.

4.3.2 Different feed compositions

It was found that the feed composition possessing high protein fraction triggered a higher flux decline rate and lower FR compared to low protein fraction, as shown in Fig. 5-a. To elucidate the results given in section 4.2, the CPs effect and the fouling resistance from these fouling cases were quantified. Generally, the extent of ICP, ECPs in a membrane fouled by low protein fraction was comparable with that by high protein fraction and this is attributed to operation at the same flux (30 LMH) and similar flux decline, particularly in the initial stage. For the initial 10 h operation

603 the flux decline rate was similar for all cases and this fact is confirmed by calculation on the fouling
604 resistance and the cake structural parameter. As presented in Fig. 8, the corresponding values for
605 fouling resistance and cake structural parameters being 2.28 $x10^{13}$ m^{-1} and 148 µm, and 2.24$x10^{13}$
606 m^{-1} and 150 µm for low and high protein fraction respectively. Clearly there is no significant
607 difference. However, it is noted that after 100 h operation the fouling resistance (3.37$x10^{13}$ m^{-1})
608 and cake structural parameter (308 µm) of membrane fouled by high protein fraction were higher
609 than those of low protein fraction i.e., 3.04$x10^{13}$ m^{-1} and 265 µm. This leads to a greater extent of
610 C-ECP for the former condition i.e., 4.96 bar, compared to the latter condition i.e., 4.30 bar. Such
611 results confirmed that a higher fouling rate occurred in the conditions of high protein fraction.
612 Generally, the cake structural parameter and the fouling resistance increased gradually for both
613 conditions. This fact implies that physical cleaning after each 20 h operation did not prevent an
614 accumulation of foulant on the membrane surface. The resultant cake layers promoted the effect
615 of C-ECP which was found to account for 10.9-13% of the total driving force.
616 As indicated by the result of cross-sectional analyses (Fig. 5c, d) the fouling layer of the low
617 protein fraction was slightly thicker than that of the high protein fraction. However, the latter
618 generates the higher fouling resistance and cake structural parameter. Such results imply that the
619 high protein fraction present in WW could lead to alterations in the foulant layer structure where
620 protein might strongly interact with alginate and humic acid in a complex fouling solution [23].
621 Overall these findings suggest that the fouling resistance and the cake structural parameter (rather
622 that thickness itself) are the pivotal factors in an evaluation of the extent of fouling.
623
624
625
626
627
628

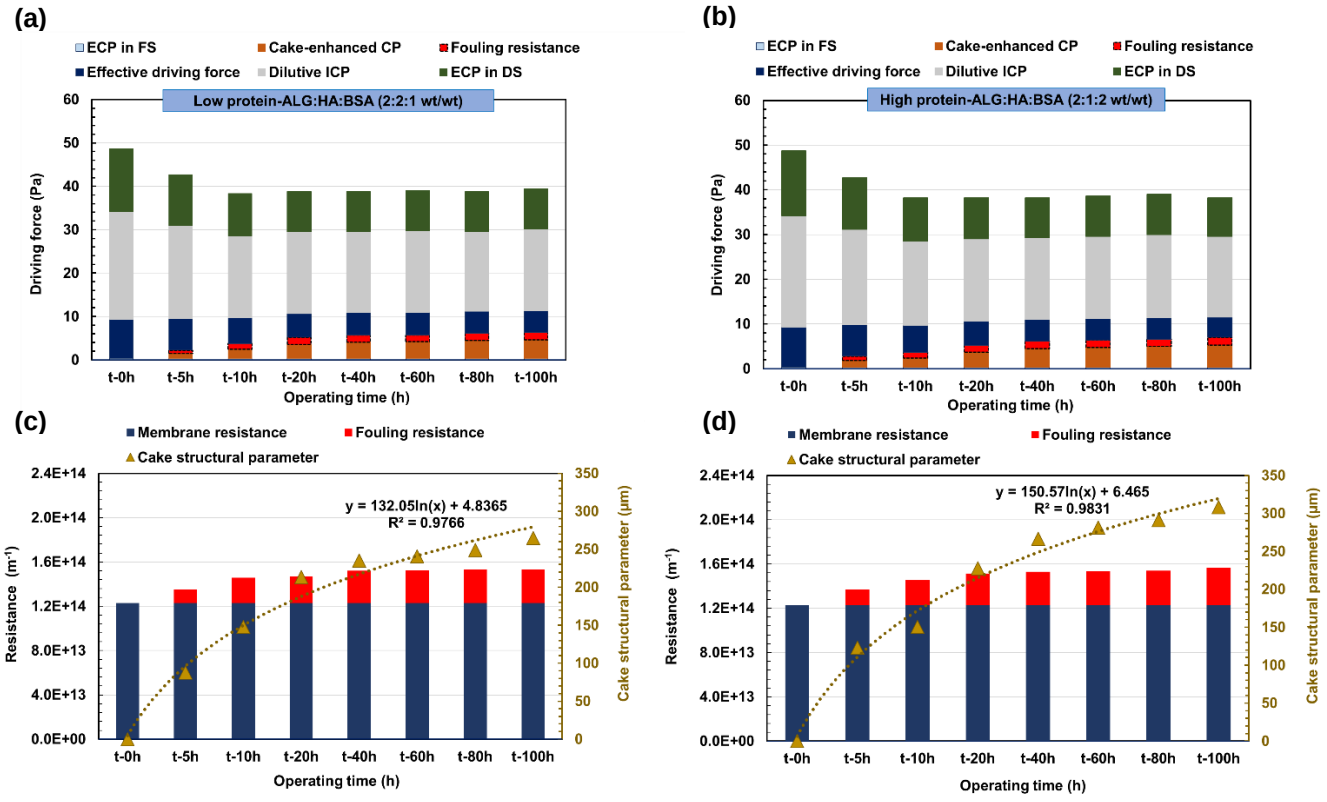

Figure 8. Change of CPs profile, cake structural parameter, and fouling resistance with different feed compositions: Low protein (a, c), high protein (b, d). A long-term fouling test was conducted for 100 h. Physical cleaning was implemented after each 20 h operation. All experiments were operated under the same flux of 30 LMH and the foulant concentration of 160 mg/L.

4.4. Correlation between factors: Cake-enhanced concentration polarization, cake structural parameter, fouling layer thickness, fouling resistance and % flux decline by fouling

This section provides an exploration of the correlation coefficients between factors i.e., cake-enhanced CP, fouling layer thickness, cake structural parameter, and fouling resistance and the flux decline rate. Table S2 presents such values of these factors under different fluxes (low, moderate, and high level), fouling time, and various foulant types (single and complex fouling). Such relationships were evaluated using Pearson's correlation coefficient (Table 2). As expected the flux decline rate showed a good correlation with the following factors: fouling layer thickness

(R= 0.897), fouling resistance (R= 0.908), cake structural parameter (R= 0.925), and cake-enhanced CP (R=0.904).

The cake structural parameter showed proficient correlations with cake-enhanced CP (R= 0.986), the fouling resistance (R=0.873). However, this was not attained between cake-enhanced CP and fouling layer thickness as their correlation coefficient was modest (0.794). These results can be probably attributed to different cake structures formed by either single or complex fouling**.** As previously reported, the tortuosity of an organic foulant cake layer was probably close to 1 [33]. If the same flux of 34 LMH was implemented (Table S-2), different cake structural parameters obtained from fouling scenarios could be due to different thickness and porosity of cake layers. Such findings suggested that the feed composition could induce a change in a cake layer-enhanced CP, fouling layer thickness, and thus pose different fouling behaviors.

As flux decline by fouling has been partially ascribed to cake layer resistance and the layer thickness, an examination to define the quantitative regression between the fouling layer thickness and the flux decline rate was made. As shown in Fig. 9, a single linear regression and logarithmic model were used for comparison. The latter model showed a stronger correlation and this was observed for the simulated WW with complex foulant (R^2= 0.9956). Notably, correlated values for simulated WW with single foulant deviated from the logarithmic regression. These findings revealed that for the feeds used the flux decline rate and fouling layer thickness can be linked through logarithimic regression analysis.

669 **Table 4.** Pearson correlation coefficient between factors such as cake-enhanced CP, cake

670 structural parameter, fouling resistance, fouling layer thickness and % flux decline by fouling

Factors	Cake-enhanced CP	Cake structural parameter	Fouling resistance	Fouling layer thickness	% Flux decline by fouling
Cake-enhanced CP	1	0.986**	0.873**	0.794*	0.904**
Cake structural parameter		1	0.928**	0.816**	0.925**
Fouling resistance			1	0.823**	0.908**
Fouling layer thickness				1	0.897**
% Flux decline by fouling					1

**. Correlation is significant at the 0.01 level (2-tailed) (n=10).

*. Correlation is moderate at the 0.05 level (2-tailed) (n=10).

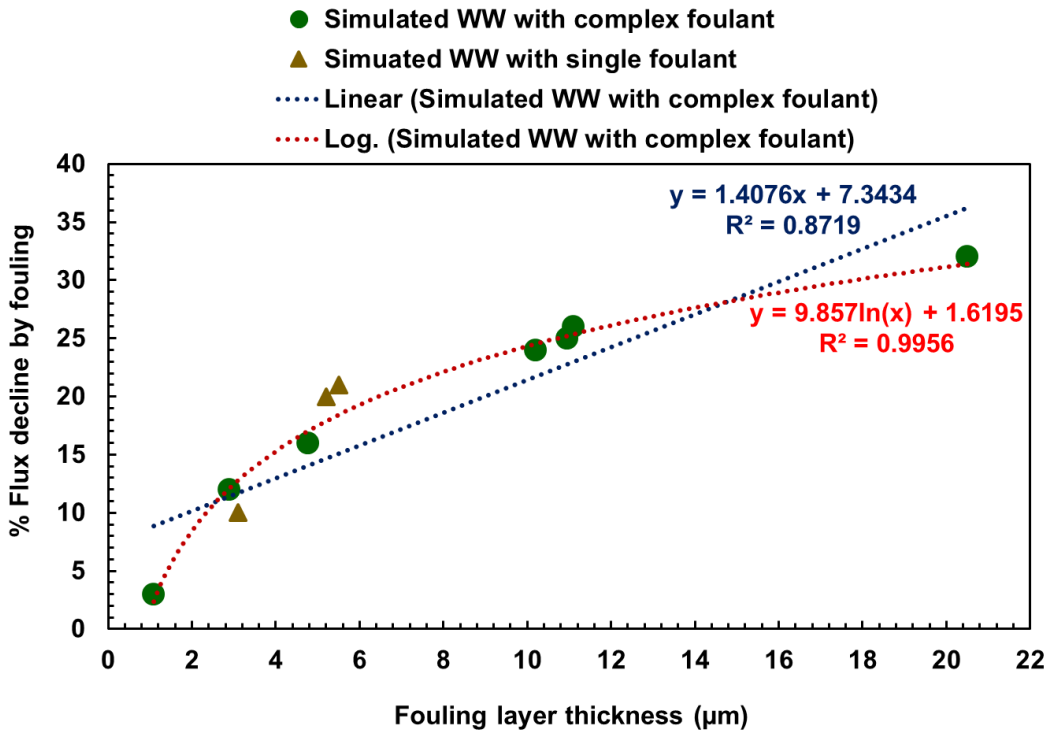

671

672 **Figure 9.** Correlation analysis between the fouling layer thickness and % flux decline by fouling

673 through linear and nonlinear regressions.

674

675

676

4.5. Implication of this research

As previously reported the raw WW/secondary WW effluents contains various types of foulants, such as proteins, polysaccharides, humic substances, and lipids, with concentration of 40-140 mg/L [41] [42]. In this study, the presence of co-organic foulants (ALG, HA, and BSA) in the feed solutions has been investigated for the FO membrane so as to give direct implications for wastewater reclamation. As illustrated in Fig. 10-g the current study reveals the critical role of choosing initial flux in organic fouling control and CPs minimization of FO operation. As indicated by the results of Fig. 10-d, e, f, after 120 h operation the greater cake layer-ECP effect was indeed observed at a high flux of 30-34 LMH whilst this fact was minor for 25 LMH. The findings highlight that the classic critical (threshold) flux applies to the osmotically driven membrane process. Herein our results for the TFC membrane suggest a threshold value of 25 LMH for a typical WW with the organic concentration of 160 mg/L.

In order to develop a guide for practical operation, a summary of studies pertaining to organic fouling of FO membranes is presented in Table 5. Such information provides a basis for the discussion and comparison with our outcomes. For a high foulant concentration (500 mg/L), severe fouling by single ALG and a low flux recovery was reported for a lab-scale TFC membrane operated under a high flux of 35.2 LMH for 100 h operation [50]. Furthermore, fouling became serious when operating with a simulated complex WW i.e., 400 mg/L concentration and at a modest flux of 16.0 LMH. This fact is attributed to foulant-foulant-membrane interactions; accelerated flux decline (43%) was observed [51]. In contrast our results indicated that a flux of 25 LMH is favorable when seeking to control fouling and minimize the effect of cake-ECP; this outcome was with a typical WW concentration of 160 mg/L. Earlier works with laboratory-scale systems are in support of this observation. Previously successful operation has been achieved with a TFC membrane and a real municipal WW with flux values of 5.0 LMH [52], 10.0 LMH [53], 20. 1 LMH [54], and 23.1 LMH [7]. However, the guideline value of 25 LMH might be inappropriate for a WWs with high concentration (400-500 mg/L). Although such concentrations

are not to be found in a real municipal WW, high strength WW is found elsewhere e.g. dairy WW or leachate WW.

The results summarized from Table 5 highlighted that the flux recovery by physical cleaning is strongly dependent on both the initial flux level and feed composition. For example, a real dairy WW containing high protein fraction posed a significant fouling i.e., flux decline by 52% and low flux restoration of 81%, even with a relatively low flux of 12.2 LMH [55]. Overall findings reinforce our observation that a proper choice of initial flux is essential for fouling control. To save on energy, cleaning, and down-time of the installation, our present work suggests that 25 LMH is a guideline for fouling control and cake-ECP minimization when operating under typical conditions characterized by TFC membrane, foulant concentration of 160 mg/L and municipal WW. Once high strength WW i.e., leachate WW, dairy WW was used for feed solution, it is of paramount importance to re-check an appropriate initial flux for FO fouling control and cake-ECP minimization.

In practice, a flux determined found from a laboratory flat sheet unit should only be used as a guide because spiral wound modules themselves may well not achieve the same level of mass transfer [38] and we note that with a pilot-scale system, fouling control was achieved with a TFC spiral wound membrane as operated at a flux of 16.6 LMH [56].

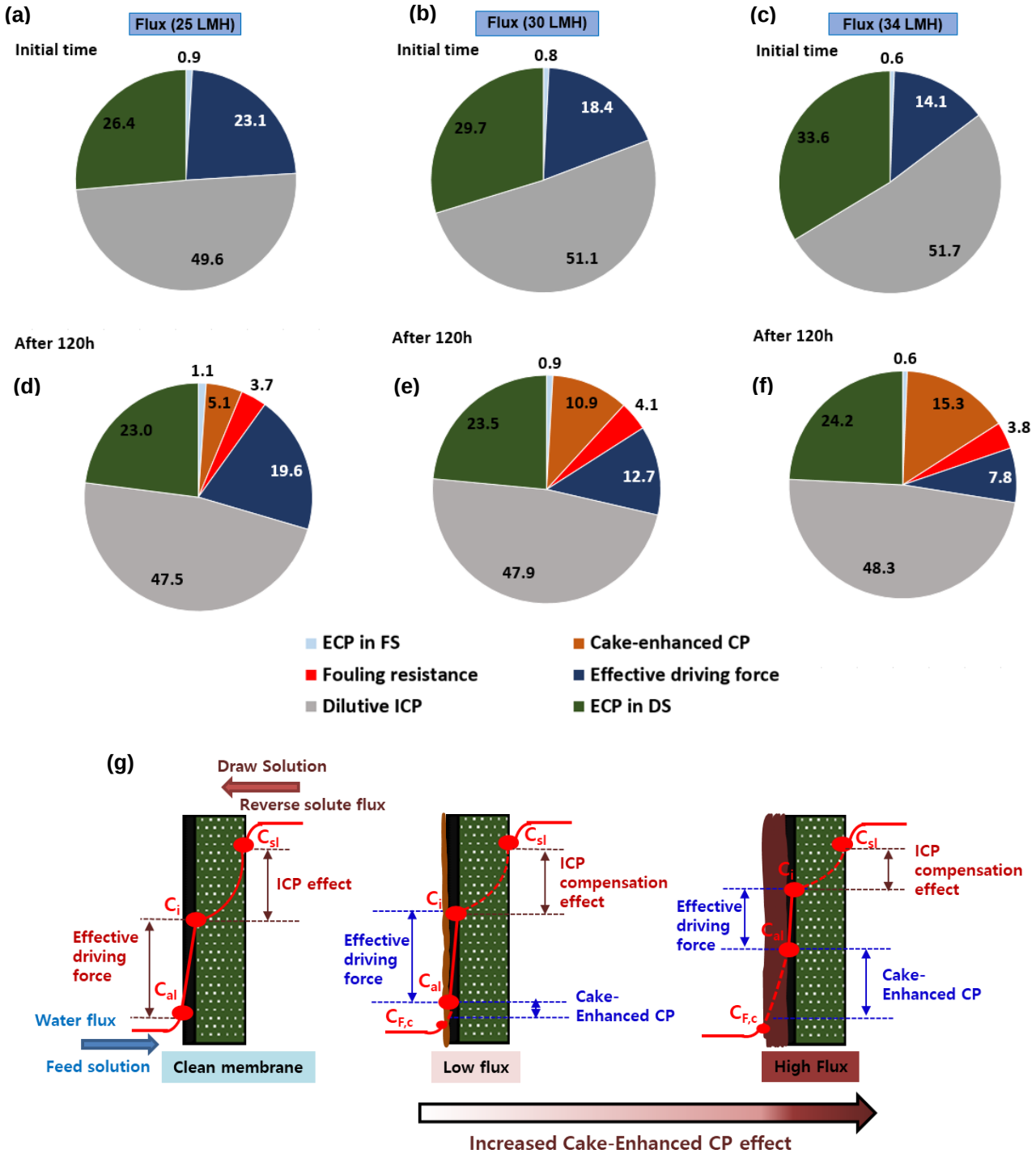

Figure 10. Contribution of the different concentration polarizations and fouling resistance on the overall driving force under different fluxes after 120 h operation: 34 LMH (a, d) either physical or chemical cleaning was conducted after each 10 h, 30 LMH (b, e) physical cleaning was conducted after 20h, 25 LMH (c, f) physical cleaning was conducted after 40 h. Diagram illustrating the FO membrane fouled by wastewater in AL-FS orientation under different fluxes (g).

736 **Table 5.** Summary of studies on organic fouling in FO membrane

Wastewater (WW)	Draw solute	Operating conditions	Initial Water flux (LMH)	Flux decline by fouling, %	Flux recovery (%)	Reference
Simulated WW with ALG 500 g/L	NaCl= 1 M	Lab-scale TFC membrane CFV= 9.6 cm/s Operating time= 100 h	35.2	25	84	[50]
Simulated WW with 200 mg/L ALG, 200 mg/L HA and 220 mg/L $CaCl_2$	Sea salt (35/L)	Lab-scale TFC membrane CFV= 10 cm/s	8.5-16	0-43	100	[51]
Secondary WW effluent	NaCl= 4%	Lab-scale TFC membrane No pretreatment CFV= 4.17 cm/s Operating time= 16 days	5.0	0	-	[52]
Municipal WW	NaCl= 5 M	Lab-scale TFC membrane Pretreatment: Coagulation, flocculation, microwaving, MF CFV= 4.17 cm/s Operating time= 4.5 h	10.0	2	-	[53]
Dairy WW	NaCl= 1 M	Lab-scale TFC membrane No pretreatment Operating time= 18 h	12.2	52	81	[55]
Municipal WW	Synthetic brine seawater	Lab-scale TFC membrane Pretreatment= MF CFV= 6.0 cm/s Operating time= 24 h	20.1	-	98	[54]
Secondary municipal WW effluent	Real seawater	Lab-scale TFC CFV= 8.5 cm/s Operating time= 80 h	23.1	5%	-	[7]
Simulated WW with 1.2 g/L sea salt, 0.22 g/L $CaCl_2$, 200 mg/L HA and 200 mg/L ALG	Sea salt (35g/L)	Pilot-scale with TFC membrane module Operating time: 3 cycles (80% recovery feed water for each cycle)	16.6	5%	-	[56]

737 Note: Flux recovery was by physical cleaning. "-" indicates absence of relevant information

738

739

740

5. Conclusions

The current work not only explored the flux decline patterns but also quantified the synergistic effect of CPs and fouling for different operating fluxes and feed compositions. The flux decline pattern was dependent on the chosen operational flux, WW composition. Notably, once a chemical cleaning was imposed, this induced a change of flux decline pattern. FO fouling was severe and more irreversible at a high flux of 34 LMH, with the formation of a cohesive and compact cake layer. Compared with operation at 25 LMH, operation at this condition triggered a four-fold increase in cake structural parameter and ten-fold increase in cake layer-enhanced CP after 40 h operation. This study confirmed that high protein fraction present in WW promoted FO fouling and caused more irreversible fouling. Based on quantitative analysis of CPs and fouling resistance, the ICP contributed most but cake layer-enhanced CP and fouling resistance had significant impact at the severe fouling condition where they were found to account for 24.5% of the overall driving force.

Acknowledgements

This work was supported by Korea Environment Industry & Technology Institute (KEITI) through Industrial Facilities & Infrastructure Research Program, funded by Korea Ministry of Environment (MOE) (1485016165). RWF was partially supported by an APEX award for Exploring Water Re-use – the Nexus of Politics, Technology and Economics. This grant was awarded by the Royal Society and British Academy and funded by the Leverhulme Trust.

Appendix A: Supplementary data

Abbreviations

ΔPc: Pressure drop caused by cake layer

μ: Water dynamic viscosity

A: water permeability coefficient

AL-FS: Active layer-facing feed solution

B: solute permeability coefficient

C_{al}: solute concentration at interface between foulant cake layer and the active layer surface

$C_{D,b}$: solute concentration of the bulk draw solution

C-ECP: cake layer-enhanced concentration polarization

CECP: concentrative external concentration polarization

$C_{F,b}$: solute concentration of the bulk feed solution

$C_{F,c}$: solute concentration on the surface of foulant cake layer

C_i: solute concentration at the interface between the active layer and the support layer

C_{sl}: solute concentration on the membrane surface of the support layer

D_c: diffusion coefficient in the cake layer

D_D: bulk diffusion coefficient of draw solution

DECP: dilutive external concentration polarization

D_F: bulk diffusion coefficient of feed solution

D_h: foulant pore hydraulic diameter

Ds: diffusion coefficient in the support layer

ECP: External concentration polarization

ICP: internal concentration polarization

J_w: water flux

k_D: mass transfer coefficient in draw side

k_F: mass transfer coefficient in feed side

RSF: reverse solute flux

S_c: foulant cake structural parameter

S_s: structural parameter of the support layer

δ_c: cake layer thickness

δ_D: thickness of the dilutive external concentration polarization in draw side

δ_F: thickness of the concentrative external concentration polarization in feed side

ε_c: cake layer porosity

ρ: Water density

τ_c: cake layer tortuosity

References

[1] M. Elimelech, W. a Phillip, The future of seawater desalination: energy, technology, and the environment., Science. (2011). doi:10.1126/science.1200488.

[2] R. Valladares Linares, Z. Li, V. Yangali-Quintanilla, N. Ghaffour, G. Amy, T. Leiknes, J.S. Vrouwenvelder, Life cycle cost of a hybrid forward osmosis - low pressure reverse osmosis system for seawater desalination and wastewater recovery, Water Res. 88 (2016) 225–234. doi:10.1016/j.watres.2015.10.017.

[3] Q. Li, Z. Xu, I. Pinnau, Fouling of reverse osmosis membranes by biopolymers in wastewater secondary effluent: Role of membrane surface properties and initial permeate flux, J. Memb. Sci. (2007). doi:10.1016/j.memsci.2006.12.027.

[4] T.Y. Cath, N.T. Hancock, C.D. Lundin, C. Hoppe-Jones, J.E. Drewes, A multi-barrier osmotic dilution process for simultaneous desalination and purification of impaired water, J. Memb. Sci. (2010). doi:10.1016/j.memsci.2010.06.056.

[5] M. Xie, L.D. Nghiem, W.E. Price, M. Elimelech, Impact of humic acid fouling on membrane performance and transport of pharmaceutically active compounds in forward osmosis, Water Res. 47 (2013) 4567–4575. doi:10.1016/j.watres.2013.05.013.

[6] Y. Sun, J. Tian, Z. Zhao, W. Shi, D. Liu, F. Cui, Membrane fouling of forward osmosis (FO) membrane for municipal wastewater treatment: A comparison between direct FO and OMBR, Water Res. 104 (2016) 330–339. doi:10.1016/j.watres.2016.08.039.

[7] F. Volpin, E. Fons, L. Chekli, J.E. Kim, A. Jang, H.K. Shon, Hybrid forward osmosis-reverse osmosis for wastewater reuse and seawater desalination: Understanding the optimal feed solution to minimise fouling, Process Saf. Environ. Prot. 117 (2018) 523–532. doi:10.1016/j.psep.2018.05.006.

[8] S.M. Iskander, S. Zou, B. Brazil, J.T. Novak, Z. He, Energy consumption by forward osmosis treatment of landfill leachate for water recovery, Waste Manag. 63 (2017) 284–291. doi:10.1016/j.wasman.2017.03.026.

[9] B. Aftab, Y.S. Ok, J. Cho, J. Hur, Targeted removal of organic foulants in landfill leachate in forward osmosis system integrated with biochar/activated carbon treatment, Water Res. 160 (2019) 217–227. doi:10.1016/j.watres.2019.05.076.

[10] S. Kook, C. Lee, T.T. Nguyen, J. Lee, H.K. Shon, I.S. Kim, Serially connected forward osmosis membrane elements of pressure-assisted forward osmosis-reverse osmosis hybrid system: Process performance and economic analysis, Desalination. (2018). doi:10.1016/j.desal.2018.09.019.

[11] C. Boo, M. Elimelech, S. Hong, Fouling control in a forward osmosis process integrating seawater desalination and wastewater reclamation, J. Memb. Sci. (2013). doi:10.1016/j.memsci.2013.05.004.

[12] C. Lee, N. Thanh, R. Syamsul, I.S. Kim, Performance analysis of serially-connected membrane element for pressure- assisted forward osmosis : wastewater reuse and seawater desalination, Desalin. Water Treat. 183 (2020) 104–113. doi:10.5004/dwt.2020.25260.

[13] C. Lee, T.-T. Nguyen, R.S. Adha, H.K. Shon, I.S. Kim, Influence of hydrodynamic operating conditions on organic fouling of spiral-wound forward osmosis membranes: Fouling-induced performance deterioration in FO-RO hybrid system, Water Res. 185 (2020) 116154. doi:10.1016/j.watres.2020.116154.

[14] M.M. Motsa, B.B. Mamba, A. D'Haese, E.M.V. Hoek, A.R.D. Verliefde, Organic fouling in forward osmosis membranes: The role of feed solution chemistry and membrane structural properties, J. Memb. Sci. 460 (2014) 99–109. doi:10.1016/j.memsci.2014.02.035.

[15] M.M. Motsa, B.B. Mamba, J.M. Thwala, A.R.D. Verliefde, Osmotic backwash of fouled FO membranes: Cleaning mechanisms and membrane surface properties after cleaning, Desalination. 402 (2017) 62–71. doi:10.1016/j.desal.2016.09.018.

[16] T. Nguyen, S. Kook, C. Lee, R.W. Field, I.S. Kim, Critical flux-based membrane fouling control of forward osmosis : Behavior , sustainability , and reversibility, J. Memb. Sci.

570–571 (2019) 380–393. doi:10.1016/j.memsci.2018.10.062.
[17] B. Mi, M. Elimelech, Chemical and physical aspects of organic fouling of forward osmosis membranes, J. Memb. Sci. 320 (2008) 292–302. doi:10.1016/j.memsci.2008.04.036.
[18] P. Zhao, B. Gao, Q. Yue, H.K. Shon, Q. Li, Fouling of forward osmosis membrane by protein (BSA): effects of pH, calcium, ionic strength, initial permeate flux, membrane orientation and foulant composition, Desalin. Water Treat. 57 (2016) 13415–13424. doi:10.1080/19443994.2015.1060539.
[19] A.W. Zularisam, A.F. Ismail, M.R. Salim, M. Sakinah, H. Ozaki, The effects of natural organic matter (NOM) fractions on fouling characteristics and flux recovery of ultrafiltration membranes, Desalination. (2007). doi:10.1016/j.desal.2006.10.010.
[20] B.G. Choi, D.I. Kim, S. Hong, Fouling evaluation and mechanisms in a FO-RO hybrid process for direct potable reuse, J. Memb. Sci. 520 (2016) 89–98. doi:10.1016/j.memsci.2016.07.035.
[21] M. Zhan, G. Gwak, D.I. Kim, K. Park, S. Hong, Quantitative analysis of the irreversible membrane fouling of forward osmosis during wastewater reclamation: Correlation with the modified fouling index, J. Memb. Sci. 597 (2020) 117757. doi:10.1016/j.memsci.2019.117757.
[22] M. Xie, L.D. Nghiem, W.E. Price, M. Elimelech, Impact of organic and colloidal fouling on trace organic contaminant rejection by forward osmosis: Role of initial permeate flux, Desalination. 336 (2014) 146–152. doi:10.1016/j.desal.2013.12.037.
[23] T.-T. Nguyen, C. Lee, R.W. Field, I.S. Kim, Insight into organic fouling behavior in polyamide thin-film composite forward osmosis membrane: critical flux and its impact on the economics of water reclamation, J. Memb. Sci. 606 (2020) 118118. doi:10.1016/j.memsci.2020.118118.
[24] F.A. Siddiqui, Q. She, A.G. Fane, R.W. Field, Exploring the differences between forward osmosis and reverse osmosis fouling, J. Memb. Sci. 565 (2018) 241–253. doi:10.1016/j.memsci.2018.08.034.
[25] J.Y. Xiong, Z.L. Cheng, C.F. Wan, S.C. Chen, T.S. Chung, Analysis of flux reduction behaviors of PRO hollow fiber membranes: Experiments, mechanisms, and implications, J. Memb. Sci. (2016). doi:10.1016/j.memsci.2016.01.012.
[26] C.Y. Tang, Q. She, W.C.L. Lay, R. Wang, A.G. Fane, Coupled effects of internal concentration polarization and fouling on flux behavior of forward osmosis membranes during humic acid filtration, J. Memb. Sci. 354 (2010) 123–133. doi:10.1016/j.memsci.2010.02.059.
[27] Y. Wang, M. Zhang, Y. Liu, Q. Xiao, S. Xu, Quantitative evaluation of concentration polarization under different operating conditions for forward osmosis process, DES. 398 (2016) 106–113. doi:10.1016/j.desal.2016.07.015.
[28] C. Suh, S. Lee, Modeling reverse draw solute flux in forward osmosis with external concentration polarization in both sides of the draw and feed solution, J. Memb. Sci. 427 (2013) 365–374. doi:10.1016/j.memsci.2012.08.033.
[29] E. Arkhangelsky, F. Wicaksana, C. Tang, A.A. Al-Rabiah, S.M. Al-Zahrani, R. Wang, Combined organic-inorganic fouling of forward osmosis hollow fiber membranes, Water Res. 46 (2012) 6329–6338. doi:10.1016/j.watres.2012.09.003.
[30] X. Xiang, S. Zou, Z. He, Energy consumption of water recovery from wastewater in a submerged forward osmosis system using commercial liquid fertilizer as a draw solute, Sep. Purif. Technol. 174 (2017) 432–438. doi:10.1016/j.seppur.2016.10.052.
[31] E.M.V. Hoek, M. Elimelech, Cake-Enhanced Concentration Polarization: A New Fouling Mechanism for Salt-Rejecting Membranes, Environ. Sci. Technol. 37 (2003) 5581–5588. doi:10.1021/es0262636.
[32] L. Zheng, W.E. Price, L.D. Nghiem, Effects of fouling on separation performance by forward osmosis: the role of specific organic foulants, Environ. Sci. Pollut. Res. (2018) 1–

12. doi:10.1007/s11356-018-2277-7.
[33] E. Nagy, I. Hegedüs, E.W. Tow, J.H. Lienhard V, Effect of fouling on performance of pressure retarded osmosis (PRO) and forward osmosis (FO), J. Memb. Sci. 565 (2018) 450–462. doi:10.1016/j.memsci.2018.08.039.
[34] E.W. Tow, J.H. Lienhard, Quantifying osmotic membrane fouling to enable comparisons across diverse processes, J. Memb. Sci. 511 (2016) 92–107. doi:10.1016/j.memsci.2016.03.040.
[35] W.A. Phillip, J.S. Yong, M. Elimelech, Reverse draw solute permeation in forward osmosis: Modeling and experiments, Environ. Sci. Technol. 44 (2010) 5170–5176. doi:10.1021/es100901n.
[36] R.W. Field, J.J. Wu, Mass transfer limitations in forward osmosis: Are some potential applications overhyped?, Desalination. 318 (2013) 118–124. doi:10.1016/j.desal.2013.01.025.
[37] N.N. Bui, J.T. Arena, J.R. McCutcheon, Proper accounting of mass transfer resistances in forward osmosis: Improving the accuracy of model predictions of structural parameter, J. Memb. Sci. 492 (2015) 289–302. doi:10.1016/j.memsci.2015.02.001.
[38] R.W. Field, F.A. Siddiqui, P. Ang, J.J. Wu, Analysis of the influence of module construction upon forward osmosis performance, Desalination. 431 (2017) 151–156. doi:10.1016/j.desal.2017.09.003.
[39] E.W. Tow, M.M. Rencken, J.H. Lienhard, In situ visualization of organic fouling and cleaning mechanisms in reverse osmosis and forward osmosis, Desalination. 399 (2016) 138–147. doi:10.1016/j.desal.2016.08.024.
[40] A. Tiraferri, N.Y. Yip, A.P. Straub, S.R. Castrillon, A method for the simultaneous determination of transport and structural parameters of forward osmosis membranes, J. Memb. Sci. 444 (2013) 523–538. doi:10.1016/j.memsci.2013.05.023.
[41] M. Wang, Y. Chen, Generation and characterization of DOM in wastewater treatment processes, Chemosphere. 201 (2018) 96–109. doi:10.1016/j.chemosphere.2018.02.124.
[42] M. Huang, Y. Li, G. Gu, Chemical composition of organic matters in domestic wastewater, DES. 262 (2010) 36–42. doi:10.1016/j.desal.2010.05.037.
[43] N. Vakondios, E.E. Koukouraki, E. Diamadopoulos, Effluent organic matter (EfOM) characterization by simultaneous measurement of proteins and humic matter, Water Res. 63 (2014) 62–70. doi:10.1016/j.watres.2014.06.011.
[44] Q. She, X. Jin, Q. Li, C.Y. Tang, Relating reverse and forward solute diffusion to membrane fouling in osmotically driven membrane processes, Water Res. 46 (2012) 2478–2486. doi:10.1016/j.watres.2012.02.024.
[45] R.W. Field, J.J. Wu, On boundary layers and the attenuation of driving forces in forward osmosis and other membrane processes, Desalination. 429 (2018) 167–174. doi:10.1016/j.desal.2017.12.001.
[46] Z. Wang, J. Tang, C. Zhu, Y. Dong, Q. Wang, Z. Wu, Chemical cleaning protocols for thin film composite (TFC) polyamide forward osmosis membranes used for municipal wastewater treatment, J. Memb. Sci. 475 (2015) 184–192. doi:10.1016/j.memsci.2014.10.032.
[47] A. Simon, W.E. Price, L.D. Nghiem, Influence of formulated chemical cleaning reagents on the surface properties and separation efficiency of nanofiltrationmembranes, J. Memb. Sci. (2013). doi:10.1016/j.memsci.2012.12.029.
[48] R.W. Field, G.K. Pearce, Critical, sustainable and threshold fluxes for membrane filtration with water industry applications, Adv. Colloid Interface Sci. 164 (2011) 38–44. doi:10.1016/j.cis.2010.12.008.
[49] Q. She, R. Wang, A.G. Fane, C.Y. Tang, Membrane fouling in osmotically driven membrane processes: A review, J. Memb. Sci. 499 (2016) 201–233. doi:10.1016/j.memsci.2015.10.040.
[50] J. Jung, J. Ryu, Y. Yu, J. Kweon, Characteristics of organic fouling, reversibility by

physical cleaning and concentrates in forward osmosis membrane processes for wastewater reclamation, Chemosphere. 245 (2020) 125787. doi:10.1016/j.chemosphere.2019.125787.
[51] G. Blandin, H. Vervoort, P. Le-Clech, A.R.D. Verliefde, Fouling and cleaning of high permeability forward osmosis membranes, J. Water Process Eng. 9 (2016) 161–169. doi:10.1016/j.jwpe.2015.12.007.
[52] Z. Li, R. Valladares Linares, S. Bucs, L. Fortunato, C. Hélix-Nielsen, J.S. Vrouwenvelder, N. Ghaffour, T.O. Leiknes, G. Amy, Aquaporin based biomimetic membrane in forward osmosis: Chemical cleaning resistance and practical operation, Desalination. 420 (2017) 208–215. doi:10.1016/j.desal.2017.07.015.
[53] T. Hey, N. Bajraktari, J. Vogel, C. Hélix Nielsen, J. la Cour Jansen, K. Jönsson, The effects of physicochemical wastewater treatment operations on forward osmosis, Environ. Technol. (United Kingdom). 38 (2017) 2130–2142. doi:10.1080/09593330.2016.1246616.
[54] S. Yang, B. Gao, A. Jang, H. kyong Shon, Q. Yue, Municipal wastewater treatment by forward osmosis using seawater concentrate as draw solution, Chemosphere. 237 (2019) 124485. doi:10.1016/j.chemosphere.2019.124485.
[55] H. Song, F. Xie, W. Chen, J. Liu, FO/MD hybrid system for real dairy wastewater recycling, Environ. Technol. (United Kingdom). 39 (2018) 2411–2421. doi:10.1080/09593330.2017.1377771.
[56] J. Kim, G. Blandin, S. Phuntsho, A. Verliefde, P. Le-clech, H. Shon, Practical considerations for operability of an 8 ″ spiral wound forward osmosis module : Hydrodynamics , fouling behaviour and cleaning strategy, DES. 404 (2017) 249–258. doi:10.1016/j.desal.2016.11.004.